

REVIEW

Open Access



# Optical polarization manipulations with anisotropic nanostructures

Zhancheng Li<sup>1</sup>, Wenwei Liu<sup>1</sup>, Yuebian Zhang<sup>1</sup>, Hua Cheng<sup>1\*</sup>, Shuang Zhang<sup>3\*</sup> and Shuqi Chen<sup>1,2,4\*</sup> 

\*Correspondence:  
hcheng@nankai.edu.cn;  
shuzhang@hku.hk;  
schen@nankai.edu.cn

<sup>1</sup>The Key Laboratory of Weak Light Nonlinear Photonics, Ministry of Education, School of Physics and TEDA Institute of Applied Physics, Nankai University, Tianjin 300071, China

<sup>2</sup>School of Materials Science and Engineering, Smart Sensing Interdisciplinary Science Center, Nankai University, Tianjin 300350, China

<sup>3</sup>New Cornerstone Science Laboratory, Department of Physics, The University of Hong Kong, Pokfulam, Hong Kong, China

<sup>4</sup>The Collaborative Innovation Center of Extreme Optics, Shanxi University, Taiyuan 030006, Shanxi, China

## Abstract

Over the past few decades, metasurfaces have revolutionized conventional bulky optics by providing an effective approach to manipulate optical waves at the subwavelength scale. This advancement holds great potential for compact, multifunctional, and reconfigurable optical devices. Notably, metasurfaces constructed with anisotropic nanostructures have exhibited remarkable capability in manipulating the polarization state of optical waves. Furthermore, they can be employed to achieve independent control of the amplitude and phase of optical waves in different polarization channels. This capability has garnered significant attention from the photonics community due to its unprecedented potential for polarization-selective and -multiplexed optical wave manipulation, offering versatile applications in optical imaging, communication, and detection. This paper reviews the design principles, representative works, and recent advancements in anisotropic nanostructures for optical polarization manipulation, detection, as well as polarization-selective and -multiplexed optical wave manipulation. Personal insights into further developments in this research area are provided.

**Keywords:** Metasurface, Anisotropic nanostructures, Optical wave manipulation, Polarization-multiplexed manipulation

## Introduction

Polarization, a fundamental characteristic of optical waves, plays a pivotal role in the field of optical imaging and communication [1, 2]. It holds great potential for advanced optical multiplexing and multi-functional integration, as the amplitude and phase of optical waves with orthogonal polarization states can be independently manipulated. Conventional optical elements for polarization manipulation are typically made from materials exhibiting optical dichroism. These materials can introduce controlled phase delays between two orthogonally polarized electric fields by adjusting the optical wave propagation distance. Despite their effectiveness in controlling polarization, conventional optical elements often suffer from bulkiness and limited functionality. This makes them less versatile and less adaptable to modern nanophotonic applications where high-precision optical polarization manipulation based on miniaturized devices is required. As such, researchers have been continuously exploring new candidates that possess

flexible capabilities for optical polarization manipulation while maintaining compactness and efficiency.

Fortunately, recent advances in nanotechnology have opened exciting possibilities for creating highly functional and compact optical elements [3–7]. Metasurfaces, which are planar arrays consisting of subwavelength artificial nanostructures, have been demonstrated as excellent candidates for optical wave manipulation with high efficiency and superb customization [8–14]. This is because they allow for precise control over optical responses through adjustments of structural parameters [15, 16]. Metasurfaces consisting of periodically arranged anisotropic nanostructures can induce distinct phases on orthogonal linear polarizations, rendering them a potent platform for optical polarization manipulation. The investigation of high-performance optical polarization control devices based on anisotropic nanostructures, including polarizers, wave plates, polarization converters, and selectors, has been extensively conducted in recent years [17–28]. Moreover, anisotropic nanostructures can be utilized to independently manipulate the phase and amplitude of optical waves with orthogonal polarization states at the subwavelength scale, serving as a fertile ground for polarization-selective and -multiplexed optical wave manipulation [29–38]. The exceptional capability of anisotropic nanostructures for polarization-selective optical wave manipulation has significant applications in detecting the polarization states of optical waves [39–43]. Recent progress on metasurfaces composed of few-layer and polyatomic anisotropic nanostructures further proved the great potential of anisotropic nanostructures for high-efficiency polarization-multiplexed full-space optical wave manipulation [44–48]. The multiplexed channels now encompass not only orthogonal linear and circular polarization states but also arbitrary and non-orthogonal states, significantly enhancing their versatility [49–51]. As research continues to improve the efficiency and flexibility of anisotropic nanostructures, we anticipate significant advancements in polarization-multiplexed optical wave manipulation in the coming years.

Herein, we review the representative works and recent advancements in anisotropic nanostructures for optical polarization manipulation, detection as well as polarization-selective and -multiplexed optical wave manipulation. We present a concise overview of the field's progress, as illustrated in Fig. 1. This article is organized into five main sections: In Section "[The design principle of anisotropic nanostructures](#)", we briefly discuss the design principle of anisotropic nanostructures. A range of representative works that have utilized anisotropic structures to achieve optical polarization manipulation and polarization-selective optical wave manipulation are discussed in Section "[Optical polarization manipulation and polarization-selective optical wave manipulation based on anisotropic nanostructures](#)". Additionally, a review of methods for measuring optical polarization state using anisotropic nanostructures is provided in Section "[Optical polarization state measurement based on anisotropic nanostructures](#)". Moreover, we provide an in-depth analysis of recent advancements in few-layer and polyatomic anisotropic nanostructures for polarization-selective and -multiplexed optical wave manipulation in Section "[Polarization-multiplexed optical wave manipulation based on few-layer and polyatomic metasurfaces composed of anisotropic nanostructures](#)", highlighting their impressive versatility and efficiency. The final section offers a conclusion and an outlook, which present our opinions on the future developments of this research area.

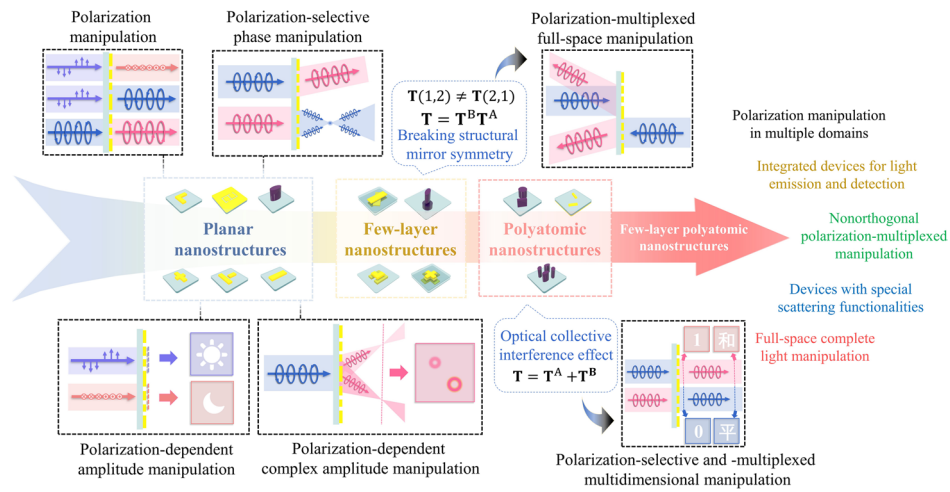


**Fig. 1** Development of anisotropic nanostructures and their utilization in polarization-selective and -multiplexed optical wave manipulation. Few-layer and polyatomic nanostructures offer greater design flexibility compared to planar nanostructures, making them powerful platforms for polarization-selective and -multiplexed full-space and multidimensional manipulation of optical waves. A detailed discussion on the advantages of few-layer and polyatomic nanostructures can be found in Section "Polarization-multiplexed optical wave manipulation based on few-layer and polyatomic metasurfaces composed of anisotropic nanostructures"

### The design principle of anisotropic nanostructures

The polarization state of a plane wave propagating in the positive  $z$  direction is determined by the temporal evolution of the electric-field vector  $\mathbf{E}(\mathbf{r}, t)$ , which can be decomposed into two orthogonal polarization components and is typically expressed using a linear basis [52]:

$$\mathbf{E}(\mathbf{r}, t) = \begin{pmatrix} E_x \\ E_y \end{pmatrix} = \begin{pmatrix} a_x e^{i\varphi_x} \\ a_y e^{i\varphi_y} \end{pmatrix} e^{i(\omega t - kz)} \quad (1)$$

where  $\omega$  and  $k$  represent the frequency and the wave vector of the plane wave, respectively, while  $a_x$  ( $a_y$ ) and  $\varphi_x$  ( $\varphi_y$ ) denote the amplitude and phase of the electric-field. The endpoint of the vector  $\mathbf{E}(\mathbf{r}, t)$  is an ellipse characterized by the azimuth angle  $\psi$  and the ellipticity angle  $\chi$ , which can be obtained from the expressions [26]:

$$\tan(2\psi) = \frac{2r}{1 - r^2} \cos(\Delta\varphi) \quad (2a)$$

$$\sin(2\chi) = \frac{2r}{1 + r^2} \sin(\Delta\varphi) \quad (2b)$$

where  $r = a_y/a_x$  and  $\Delta\varphi = \varphi_y - \varphi_x$ . The azimuth angle  $\psi$  determines the orientation angle of the polarization ellipse while the ellipticity angle  $\chi$  determines the shape of the polarization ellipse. The polarization state of optical waves can be manipulated at will by independently modulating the amplitude and phase of their two orthogonal polarization

components, which also allows for optical multiplexing in two orthogonal polarization channels. To meet this requirement, a customizable anisotropic optical response is essential.

For artificial nanostructures at the subwavelength scale, the electric fields of the normal incident ( $\mathbf{E}^i$ ) and transmitted waves ( $\mathbf{E}^o$ ) can be connected by using the Jones matrix ( $\mathbf{E}^o = \mathbf{T} \cdot \mathbf{E}^i$ ) [53]:

$$\begin{pmatrix} E_x^o \\ E_y^o \end{pmatrix} = \begin{pmatrix} T_{xx} & T_{xy} \\ T_{yx} & T_{yy} \end{pmatrix} \begin{pmatrix} E_x^i \\ E_y^i \end{pmatrix} \quad (3)$$

When the nanostructure is rotated along the  $z$ -axis with an angle of  $\theta$ , its  $T$  matrix can be obtained based on  $\mathbf{T}^\theta = \mathbf{R}(-\theta)\mathbf{TR}(\theta)$ , where  $\mathbf{R}$  is a  $2 \times 2$  rotation matrix [54]. The matrix  $T$  is represented using a linear basis here, and can be transformed into other bases as well [52]. The electric fields of the incident and reflected waves can also be connected in a similar manner [44, 55]. Then, a metasurface composed of arranged nanostructures can be described by a spatially-varying  $T$  matrix  $\mathbf{T}(x, y)$ , and the far-field distribution of optical waves can be obtained by  $\mathbf{A}(k_x, k_y) = \mathcal{F}\{\mathbf{T}(x, y)\}$  [56]. The complex coefficients of the  $T$  matrix can be well adjusted by altering the structural symmetry of nanostructures and modulating the excitation and coupling of optical resonances within them. This allows customizable anisotropic optical responses, facilitating efficient manipulation of the polarization state of optical waves. It is possible to effectively manipulate not only the polarization state of transmitted waves but also the phase and amplitude of the two orthogonal polarization components by designing the Jones matrix  $\mathbf{T}(x, y)$  of metasurfaces. For instance, if the four complex coefficients of the Jones matrix  $\mathbf{T}(x, y)$  can be independently manipulated, optical multiplexing with four polarization channels can be achieved by controlling the polarization state of the incident wave and detecting distinct polarization components of the transmitted wave. However, there are two major challenges to implementing this goal. Firstly, it is important to consider the structural symmetry when designing a nanostructure to achieve a desired  $T$  matrix. For example, the values of  $T_{xy}$  and  $T_{yx}$  are always equal when the designed nanostructure has a mirror symmetry in the  $x$ - $y$  plane [52]. Meanwhile, in order to modulate the complex coefficients of the  $T$  matrix on a larger scale, further improvements are required in the adjustable degree of freedom of structural parameters. Therefore, the design of metasurfaces composed of nanostructures with different anisotropic optical responses can be divided into the following steps: (1) Determine the  $T$  matrix of every nanostructure based on  $\mathbf{T}(x, y)$  or  $\mathbf{A}(k_x, k_y)$ ; (2) Determine the structural symmetry constraint of the nanostructures; (3) Design and find the nanostructures with desired  $T$  matrix by varying the structural parameters. If only one or two coefficients in the  $T$  matrix need to be adjusted, simple nanostructures will suffice. However, if more coefficients require modulation, nanostructures with low structural symmetry and multiple adjustable parameters are necessary. To simplify the design process of nanostructures, few-layer and polyatomic nanostructures have been proposed [47]. The coefficients in the Jones matrices of few-layer and polyatomic nanostructures can be flexibly manipulated. As illustrated in Fig. 1, few-layer nanostructures allow for easy breaking of structural mirror symmetry and involve more adjustable structural parameters. The Jones matrix of few-layer

nanostructures can be obtained by taking the dot product of each layer's Jones matrix, when the interlayer interactions are negligible. For polyatomic nanostructures, multiple different nanostructures are placed in one subwavelength unit cell, which significantly expands the adjustable structural parameters. The Jones matrix of polyatomic nanostructures can be obtained by directly adding the Jones matrices of the multiple nanostructures when the near neighbor interactions between them are negligible. Meanwhile, few-layer metasurface with independently designed Jones matrices for each layer and a much larger distance between layers than the operational wavelength has also been demonstrated as an effective alternative to achieve any desired  $\mathbf{T}(x, y)$  [57]. Note that while few-layer and polyatomic metasurfaces have emerged as efficient approaches for manipulating multiple coefficients in the  $T$  matrix, the increased number of structural parameters complicates the design and optimization process. Consequently, optimization techniques such as genetic algorithms and particle swarm optimization have been widely employed to determine the structural parameters of nanostructures [58, 59]. Meanwhile, the development of deep-learning technology also benefits the design of nanostructures with desired Jones matrices [60–65]. By combining advanced optimization techniques with the aforementioned design principles, the design of nanostructures for optical polarization manipulation and polarization-multiplexed optical wave manipulation will become faster and more efficient.

### **Optical polarization manipulation and polarization-selective optical wave manipulation based on anisotropic nanostructures**

#### ***Optical polarization manipulation***

Anisotropic nanostructures are promising candidates for subwavelength optical polarization manipulation since the complex coefficients in their transmission and reflection matrices can be easily adjusted. For instance, to function as a linear polarizer under normal illumination of plane waves (supposing optical waves propagate along the  $z$  axis), the transmission (Jones) matrix  $T$  of the designed nanostructure should have two cross-polarized coefficients ( $T_{xy}$  and  $T_{yx}$ ) and one of the two co-polarized coefficients ( $T_{xx}$  or  $T_{yy}$ ) that are close to zero. For nanostructures that is mirror-symmetric with respect to the  $x$ - $z$  or  $y$ - $z$  plane, both two cross-polarized coefficients ( $T_{xy}$  and  $T_{yx}$ ) are always equal to zero. Additionally, one of the two co-polarized coefficients ( $T_{xx}$  or  $T_{yy}$ ) can be adjusted to zero by involving an optical resonance that can be excited solely by  $x$ - or  $y$ -polarized waves. Hence, the metallic nanorod, which has an electric dipole resonance that can be excited by the component of the electric field along its structural long axis, is widely used as a near-perfect linear polarizer at the resonant wavelength [66–68]. For nanostructures composed of multiple nanorods, the working waveband can be further expanded due to the coupling of the electric dipole resonances [67]. However, the extinction ratios of these kind of designs are limited by the finite resonance strength in planar nanostructures. Recently, a bilayer metasurface made up of aluminum nanorods (shown in Fig. 2(a)) has been shown to be an excellent linear polarizer with significantly improved extinction ratio and working bandwidth compared to a single layer design consisting of aluminum nanorods with the same structural parameters [70]. Due to the enhanced optical resonance caused by the multiple wave interference effect between the layers, the working efficiency of the bilayer metasurface is greater than 90% with the

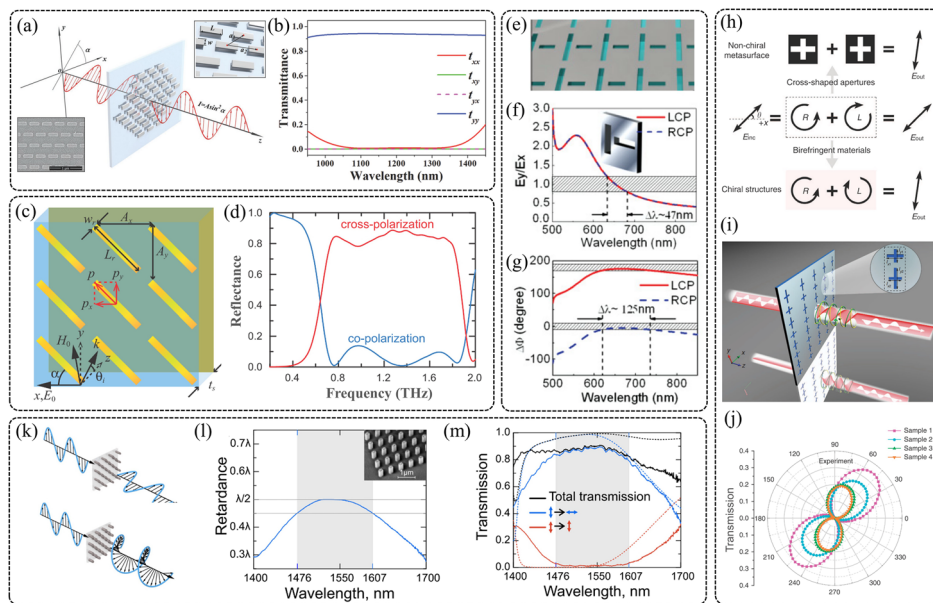


**Fig. 2** Optical polarization manipulation based on anisotropic nanostructures. **a** Schematic diagram of a bilayer metasurface consisting of aluminum nanorods functioning as a broadband perfect linear polarizer. **b** The magnitudes squared of the four transmission coefficients in the transmission matrix of the bilayer metasurface. **c** Schematic of a broadband linear polarization converter, comprising a cut-wire array, a polyimide dielectric spacer, and a gold ground plane. **d** Experimentally measured co- and cross-polarized reflectance. **e** An illustration of a nanoslit plasmonic metasurface. **f** Amplitude ratio and **g** phase difference of transmitted field  $E_x$  and  $E_y$  for the nanoslit plasmonic metasurface. **h** Comparison between conventional method and a non-chiral plasmonic metasurface consisting of two cross-shaped nanoapertures with different structural parameters for controllable optical activity. **i** Schematic of the non-chiral plasmonic metasurface for the realization of optical activity. Inset: unit cell of the non-chiral plasmonic metasurface. **j** Experimental measured transmittances as a function of analyzer angle for four non-chiral plasmonic metasurfaces with varying optical rotation angles. **k** Schematic of dielectric metasurfaces operating as highly efficient half- and quarter-wave plates. **l** Phase retardance of the half-wave plate. **m** Experimental (solid lines) and theoretical (dashed lines) transmission spectra of the half-wave plate. **a, b** adapted from Ref. [70], Copyright 2019, with permission from Wiley–VCH Verlag GmbH & Co. KGaA, Weinheim. **c, d** adapted from Ref. [79], Copyright 2013, with permission from American Association for the Advancement of Science. **e, f, g** adapted from Ref. [80], Copyright 2011, with permission from American Physical Society. **h, i, j** adapted from Ref. [81], Copyright 2016, with permission from Springer Nature, under a Creative Commons Attribution 4.0 International License. **k, l, m** adapted from Ref. [84], Copyright 2016, with permission from American Institute of Physics

extinction ratio more than 98% for wavelength from 1050 to 1350 nm, as illustrated in Fig. 2(b). This design can also be treated as a linear polarization selector, allowing  $y$ -polarized waves to pass through while blocking  $x$ -polarized waves. Similarly, a circular polarization selector can be achieved by setting the two cross-polarized coefficients ( $T_{LR}$  and  $T_{RL}$ ) and one of the two co-polarized coefficients ( $T_{LL}$  or  $T_{RR}$ ) to zero [28]. Besides their use in selecting polarization, nanostructures can also manipulate the polarization state of transmitted waves by adjusting both co- and cross-polarized coefficients within their transmission matrices. An example of this would be the achievement of cross-polarization conversion for linearly polarized waves, which requires the amplitude of  $T_{xx}$  (or  $T_{yy}$ ) equal zero while maximizing that of  $T_{yx}$  (or  $T_{xy}$ ) [71–79]. The performance of these cross-polarization converters has been evaluated by using the polarization conversion rate (PCR) defined as  $\text{PCR} = T_{ji}^2 / (T_{ii}^2 + T_{ji}^2)$ , where the subscript “ $i$ ” and “ $j$ ”

represent two orthogonal linear polarization states. Assuming the illumination is an  $x$ -polarized wave, achieving a high PCR using metallic nanostructures with electric resonances requires eliminating the  $x$ -component of the electric resonances and enhancing the strength of their  $y$ -component. In this way, a metasurface consisting of two rotationally symmetric “F” shapes connected by a central line has been proposed to achieve cross-polarization conversion in the THz range with a PCR exceeding 90% [76]. Despite the high value of PCR, the cross-polarized coefficients in the transmission matrix of this design have an amplitude lower than 0.3, indicating a working efficiency below 10%. Bilayer nanostructures with abundant interlayer interactions has been widely used to realize cross-polarization conversion of linear-polarized waves with high PCR and high working efficiency [77–79]. A high-performance broadband linear polarization converter consisting of a metallic cut-wire and a metallic ground plane separated by a dielectric spacer has been implemented, as illustrated in Fig. 2(c) [79]. An electric dipole oscillated along the cut-wire can be excited under  $x$ -polarized normal incidence. The incident electric field and the  $x$ -component of the electric dipole determine the co-polarized reflected field while the  $y$ -component of the electric dipole determine the cross-polarized reflection. Without the metal ground plane, the PCR is low. However, by taking advantage of the multiple wave interference effect between the layers, the co-polarized reflectance can be reduced while the cross-polarized reflectance can be enhanced. This results in a high PCR and high reflectance of cross-polarized waves, as shown in Fig. 2(d). The PCR can be further controlled by adjusting the spacing between the metal ground plane and the cut-wire, as the multiple wave interference effect is primarily determined by this spacing. By simultaneously adjusting the amplitude of both co- and cross-polarized coefficients and their phase difference, nanostructures can also realize linear-to-circular polarization conversion [24]. Indeed, by adjusting both the co- and cross-polarized coefficients of nanostructures simultaneously, it is possible to manipulate the polarization states of outgoing waves arbitrarily when the polarization state of incidence is known. Since any polarization state can be decomposed into two orthogonal polarization components, a more intuitive approach to manipulating the polarization state of an optical wave is by using two nanostructures with optical resonances excited under two orthogonal polarization states. For instance, a plasmonic metasurface consisting of orthogonal arrays of nanoslits was demonstrated as a linear-to-circular polarization converter at the working waveband, as shown in Fig. 2(e) to (g) [80]. Two distinct resonances can be excited along the two orthogonal nanoslits respectively, resulting in the precise  $\pi/2$  phase shift between the  $x$ - and  $y$ -polarized components of transmitted waves while maintaining equal amplitude. It should be noted that the conversion from linear to circular polarization can also be achieved by utilizing single anisotropic nanostructures, wherein two electric resonances with adjacent resonant wavelengths can be excited in two orthogonal directions, respectively [26]. Similarly, a non-chiral plasmonic metasurface whose unit cell composed of two cross-shaped nanoapertures with different structural parameters has been proposed to realize controllable optical activity [81]. The two cross-shaped nanoapertures are used to manipulate the phase and amplitude of the right- and left-handed circular polarization (RCP and LCP) components of the linearly polarized light respectively, leading to the rotation of polarization direction, as illustrated in Fig. 2(h) and (i). By simply changing the

structural parameters of the two cross-shaped nanoapertures, the optical rotation angles can be well modulated from 0 to 45 degrees, as shown in Fig. 2(j). Despite the notable advancements in single-layer plasmonic metasurfaces for optical polarization manipulation, their interaction with optical waves remains constrained by their subwavelength thickness. This limitation hinders the simultaneous generation of both electric and magnetic resonances, posing a significant challenge in efficiently achieving a phase delay of  $\pi$  between two orthogonal polarization components. As a result, single-layer plasmonic metasurfaces cannot function as high-efficiency half-wave plates [82]. To overcome this drawback, one solution is to employ a few-layer design, while another option involves utilizing dielectric nanostructures [18, 83, 84]. The metal–insulator–metal (MIM) design, comprising a metallic nanostructure, a lossless dielectric spacer, and a metallic ground plane, is widely employed to achieve half-wave plates based on anisotropic plasmonic nanostructures due to the advantageous multi-wave interference effect. For example, a MIM nanostructure has been theoretically and experimentally demonstrated as a wide field of view (FOV) half-wave plate covering  $\pm 40^\circ$  in the wavelength range of 640 to 1290 nm [18]. Meanwhile, dielectric nanostructures with versatile electric and magnetic Mie resonances are free from ohmic loss, which have emerged as efficient candidates for optical polarization manipulation [83]. For example, dielectric metasurfaces consisting of elliptical cylinders (as shown in Fig. 2(k)) have been demonstrated as highly efficient quarter-wave and half-wave plates with a wide operating bandwidth in the near-infrared regime [84]. The anisotropic optical response of elliptical cylinder allows for a phase delay of  $\pi$ , resulting in the successful implementation of a half-wave plate, as shown in Fig. 2(l) and (m). It has also been verified that plasmonic nanostructures whose height is on the scale of hundreds of nanometers can exhibit high-order electric resonances, causing a phase delay of  $\pi$  between the  $x$ - and  $y$ -polarized components of transmitted waves [85].

Furthermore, metasurfaces can also enable reconfigurable manipulation of optical polarization state by using materials with dynamically tunable optical properties [87–89]. As shown in Fig. 3(a) to (c), the polarization state of reflected wave can be dynamically modulated from LCP to RCP states with a graphene-loaded plasmonic metasurface by changing the gate voltage applied in the graphene layer [88]. Moreover, because linearly polarized waves can be decomposed into LCP and RCP components with different phase delays between them, the polarization angle of linearly polarized waves can be dynamically manipulated by modulating the phase delay between LCP and RCP waves. As an example, dynamic polarization conversion at visible frequencies has been demonstrated based on an electrically tunable optical metasurface composed of anisotropic metallic nanostructures and liquid crystals (shown in Fig. 3(d) and (e)) [89]. The refractive index of liquid crystals can be electrically tunable, resulting in the electrically controlled phase delay between the reflected LCP and RCP waves. By simply manipulating the applied voltage, the polarization conversion angle can be finely tuned from 0 to 90 degrees. In addition to utilizing materials with dynamically tunable optical properties, the angular dispersion of nanostructures has emerged as another promising alternative for achieving dynamic manipulation of optical polarization [90, 91]. A metal–insulator–metal metasurface composed of cross-shaped resonators has been proposed to control the polarization states of reflected waves under linearly polarized incidence by varying the incident



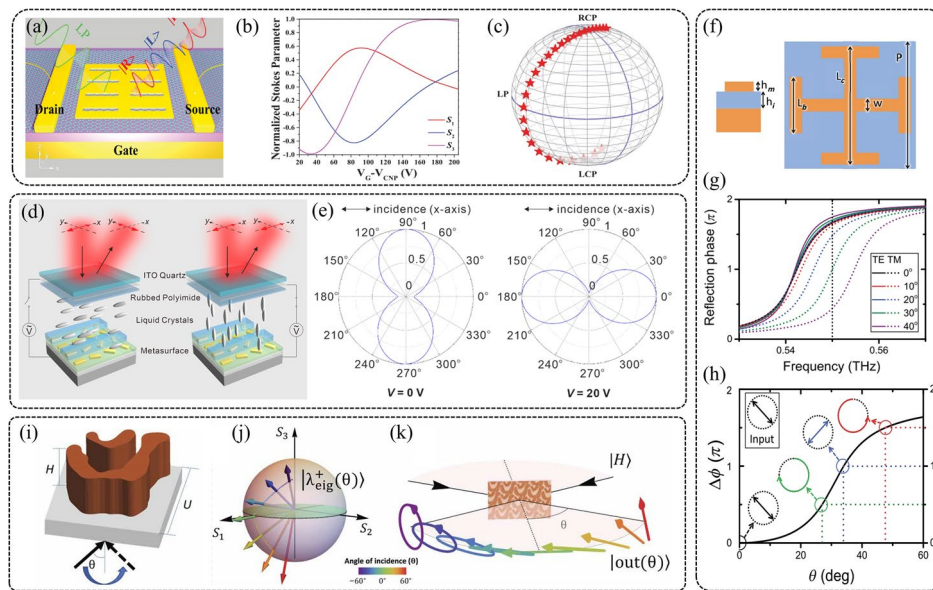


**Fig. 3** Dynamic optical polarization manipulation based on anisotropic nanostructures. **a** Schematic of a graphene-loaded plasmonic metasurface for optical polarization encoding via applying different gate voltages. **b** Variation of Normalized Stokes parameters with the modulation of the gate voltage applied on graphene. **c** The corresponding variation of polarization state on the Poincaré sphere for different Stokes parameters. **d** Dynamic optical polarization conversion based on an electrically tunable metasurface. **e** Reflectance as a function of analyzer angle for applied voltage  $V = 0$  and  $20$  V, respectively. **f** Schematic of the unit cell of the metasurface designed for polarization manipulation through control of angular dispersion. **g** Phase spectra of reflection waves under various oblique TE and TM illumination conditions. **h** The variation of phase difference between TE and TM reflected waves at  $0.55$  THz under linear-polarized oblique incidence (depicted in the inset). **i** Schematic of the unit cell of the topology-optimized metasurface. **j** Incident-angle-dependent eigen-polarization states. **k** Achieving polarization state manipulation by varying the angle of incidence while maintaining a fixed incident polarization state. **a, b, c** adapted from Ref. [88], Copyright 2015, with permission from Wiley–VCH Verlag GmbH & Co. KGaA, Weinheim. **d, e** adapted from Ref. [89], Copyright 2021, with permission from American Physical Society. **f, g, h** adapted from Ref. [90], Copyright 2018, with permission from American Physical Society. **i, j, k** adapted from Ref. [91], Copyright 2020, with permission from American Association for the Advancement of Science

angle, as illustrated in Fig. 3(f) to (h) [90]. The cross-shaped resonator exhibits a magnetic resonance at  $0.54$  THz, with the reflection phase undergoing a  $2\pi$  variation as the frequency passes through the resonant frequency. The reflection-phase spectra of the metasurface are identical under TE and TM normal incidence due to the fourfold symmetry of the cross-shaped resonator. For oblique incidence, the reflection-phase spectra for the two polarizations change in a dramatically different way, shown in Fig. 3(g). Consequently, the polarization state of reflected waves under linearly polarized incident light with a fixed polarization angle can be tuned by changing the oblique incident angle, as illustrated in Fig. 3(h). Furthermore, benefiting from the development of deep-learning technology, topology-optimized metasurfaces have been proposed to realize continuous angle-tunable birefringence, as shown in Fig. 3(i) to (k) [91]. The angle-dependent eigen-polarization states of the topology-optimized nanostructure can be artificially designed. As a result, the polarization state of reflected waves can be continuously manipulated by changing the incident angle. Recently, controlling the shearing displacement between two parallel metasurfaces acting as metagratings has been demonstrated as a novel approach for dynamically manipulating optical polarization [92]. The two metasurfaces

are composed of anisotropic dielectric nanostructures designed using freeform topology optimization to enable broadband waveplate responses. The first metasurface splits the orthogonal polarization components of the incident wave into the -1 and +1 diffraction orders, while the second metasurface diffracts and coherently recombines these beams back into the zeroth order, resulting in a normally transmitted beam. The shearing displacement between these two parallel metasurfaces introduces a phase delay between the diffracted waves, enabling dynamically tunable linear and elliptical birefringent responses. It has also been shown that the polarization state of the output wave can be dynamically controlled, scanning the full Poincaré sphere, using cascaded pairs of such parallel metasurfaces. These significant advancements highlight the importance and versatility of anisotropic nanostructures in manipulating optical polarization, which holds boundless potential for applications in integrated photonics. It is worth noting that most previous approaches focus on tailoring the state of polarization, while effective manipulation of the degree of polarization is rarely reported. In contrast, by independently adjusting the transmittance of two orthogonally polarized optical waves using anisotropic nanostructures, it has been demonstrated that unpolarized light can be filtered into light with any prescribed state of polarization and degree of polarization [93]. This significantly expands the application of anisotropic nanostructures for optical polarization manipulation. However, realizing full and dynamic control over both the state of polarization and the degree of polarization requires further investigation.

#### ***Polarization-dependent amplitude manipulation***

Benefiting from the highly adjustable complex coefficients in the transmission and reflection matrices of nanostructures, it is easy to manipulate the amplitudes of orthogonal polarization components of optical waves [8, 94]. For instance, metasurfaces composed of bilayer aluminum nanorods has been proved as good candidates for optical intensity manipulation under linear-polarized normal incidence [70]. As we mentioned above, the bilayer nanorods act as broadband perfect linear polarizers. They allow linearly polarized waves with a polarization direction along their short axis to pass through while blocking those with a polarization direction along their long axis. Two bilayer nanorods oriented along the  $x$ - and  $y$ -directions respectively are proposed as 2-bit intensity modulation elements “01” and “10”, while bilayer cross-shaped nanorods and a substrate without any nanostructures serve as the 2-bit intensity modulation elements “00” and “11”, as depicted in Fig. 4(a). With these four basic elements, polarization-selective 2-bit intensity encoding has been implemented, as shown in Fig. 4(b). Meanwhile, assuming the angle between the long axis of the bilayer nanorods and the  $x$ -direction is  $\theta$ , the transmittance under  $x$ -polarized normal incidence can be expressed as  $I = I_t \sin^2 \theta$  based on the Malus’ law, where  $I_t$  is the transmittance when  $\theta = 90^\circ$ . Under  $x$ -polarized normal incidence, the orientation angle  $\theta$  of bilayer nanorods in different spatial positions can be adjusted to arbitrarily modulate transmission intensity at the subwavelength scale. This enables high-resolution optical grayscale imaging, as illustrated in Fig. 4(c). The intensity information can be encoded into a linear polarization profile as well based on Malus’ law. An illustration is depicted in Fig. 4(d) [95]. A single reflective metasurface is designed to generate the off-axis beams with a desired polarization profile by manipulating the phase delay between the LCP and RCP components of the off-axis beams.

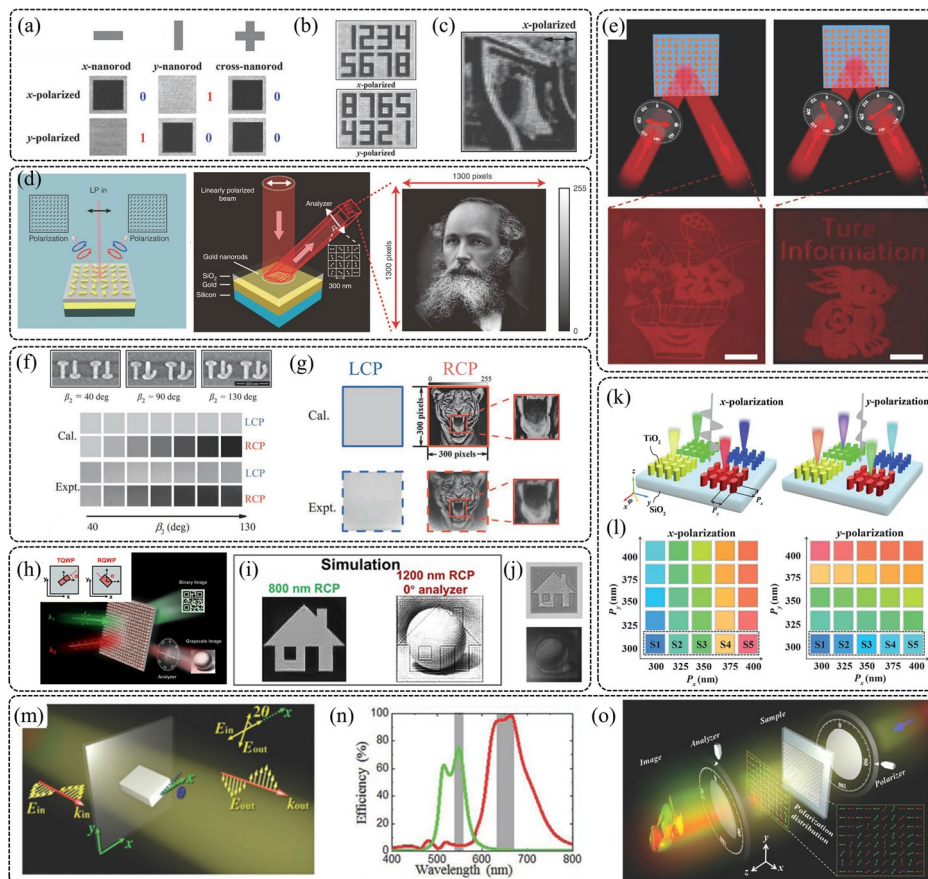


**Fig. 4** Polarization-dependent intensity manipulation based on anisotropic nanostructures. **a** Bilayer aluminum nanorods for **b** polarization-selective 2-bit intensity encoding and **c** high-resolution grayscale imaging. **d** An illustration of polarization-dependent high-resolution grayscale image based on Malus' law and plasmonic nanorods. **e** An illustration of optical encryption carrying camouflage information by utilizing dielectric anisotropic nanorods. **f** Realizing spin-selective light intensity manipulation based on diatomic umbrella-shaped nanostructures. **g** Calculated and experimentally measured 19-level grayscale tiger image at 1480 nm. **h** Schematic illustration of a double-wavelength dielectric metasurface for twofold optical display and encryption. **i** Simulated grayscale images under various input and output conditions and the **j** corresponding experimentally measured ones. **k** Schematic of dielectric metasurfaces composed of  $\text{TiO}_2$  elliptical nanopillars arranged periodically, exhibiting distinct colors under *x*- and *y*-polarized incidence. **l** Calculated reflected colors with different lattice dimensions. **m** Schematic of the polarization rotating based on a single nanoblock. **n** Calculated polarization rotating efficiency for two nanoblocks with different structural parameters. **o** Schematics of polarization encoded color image. **a**, **b**, **c** adapted from Ref. [70], Copyright 2019, with permission from Wiley–VCH Verlag GmbH & Co. KGaA, Weinheim. **d** adapted from Ref. [95], Copyright 2018, with permission from Springer Nature, under a Creative Commons Attribution 4.0 International License. **e** adapted from Ref. [96], Copyright 2022, with permission from Wiley–VCH Verlag GmbH & Co. KGaA, Weinheim. **f**, **g** adapted from Ref. [100], Copyright 2023, with permission from Wiley–VCH Verlag GmbH & Co. KGaA, Weinheim. **h**, **i**, **j** adapted from Ref. [107], Copyright 2023, with permission from De Gruyter, under a Creative Commons Attribution 4.0 International License. **k**, **l** adapted from Ref. [110], Copyright 2018, with permission from Wiley–VCH Verlag GmbH & Co. KGaA, Weinheim. **m**, **n**, **o** adapted from Ref. [116], Copyright 2018, with permission from Wiley–VCH Verlag GmbH & Co. KGaA, Weinheim

The hidden image in the generated off-axis beams can be revealed through utilization of a linear polarizer as an analyzer. By introducing both camouflage strategy and Malus' law into the design of nanostructures for manipulating optical intensity, the flexibility and capability of 2-bit polarization-selective intensity encoding based on nanostructures

can be further expanded. As illustrated in Fig. 4(e), two grayscale images corresponding to different 2-bit intensity distributions has been stored in two encryption levels, each of which can be revealed through distinct decoding conditions [96]. The key to achieving this is designing the four nanostructures that serve as fundamental coding elements based on the relationship between the intensity of reflection waves and the orientation angle  $\theta$  of nanorods under different decoding conditions [96, 97]. Recent advancements in chiral metasurfaces have further demonstrated the effectiveness of artificial nanostructures in manipulating optical intensity under circularly polarized incidence [98–100]. For example, spin-selective 2-bit intensity encoding has been well demonstrated based on chiral mirrors [99]. However, the realization of arbitrary intensity manipulation of circularly polarized waves is much more complicated since there is no such straightforward and concise law like Malus' law that can be used to guide the design of metasurfaces. Recently, a plasmonic diatomic metasurface whose unit cell consisting of two umbrella-shaped structures was proposed as a solution to this challenge [100]. As illustrated in Fig. 4(f), spin-selective full and subtle reflection intensity manipulation has been achieved by simply changing the length of the anticlockwise arc of the umbrella-shaped structure on the right side. The intensity manipulation is attributed to the modulation of the optical collective interference between the reflection waves from the two umbrella-shaped structures, which can be continuously manipulated by changing the length of the anticlockwise arc of the umbrella-shaped structure. This method enables the realization of chiral high-level grayscale imaging, as demonstrated in Fig. 4(g). The aforementioned approaches are all discussed within a single operational wavelength. However, it is also important to realize optical intensity manipulation across multiple wavelengths or a broad bandwidth in order to facilitate wavelength-multiplexed applications, structural color generation and optical encryption [101–106]. Anisotropic dielectric nanostructures with versatile polarization manipulation functionalities have been demonstrated as excellent candidates for achieving wavelength-selective optical display and encryption. As illustrated in Fig. 4(h), a dielectric metasurface composed of two types of nano bricks has been proposed to achieve dual optical display [107]. The two types of nano bricks exhibit near unity and zero transmission efficiency at 800 nm respectively, while concurrently acting as quarter-wave plates at 1200 nm. As illustrated in Fig. 4(i) and (j), a binary image and a grayscale image can be encoded into these two operational wavelengths, respectively, by utilizing these two types of nano bricks with different orientation angles. Meanwhile, Anisotropic dielectric nanostructures have been shown to be excellent candidates for creating polarization-selective structural color by adjusting their optical resonances across the entire visible spectrum [108–110]. For example, when arranging all-dielectric elliptical nanocylinders with different periods in the  $x$  and  $y$  directions to form metasurfaces, they display distinct colors under  $x$ - and  $y$ -polarized incidence, as depicted in Fig. 4(k) and (l) [110]. The anisotropic nanostructures have emerged as a good platform for the realization of polarization-selective colorful images with high resolution [111–115]. Furthermore, the color information can also be encoded into a polarization profile of the light beam. Figure 4(m) to (o) show a typical example [116]. Two dielectric nanopillars functions as half-wave plates in two adjacent wavebands are designed to generate the desired polarization profile for two different colors. The nanopillars can rotate the polarization direction of linear-polarized

waves by controlling the angle between the long axis of nanopillar and the polarization direction of linear-polarized incidence. A dielectric metasurface consisting of the two nanopillars with different orientation angles was designed to encode a color image. An additional linear polarizer (analyzer) is placed behind the metasurface to reveal the image based on the Malus' law, as shown in Fig. 4(o). This method is highly effective in adjusting color brightness, making full-color nanopainting possible [117]. Obviously, anisotropic nanostructures show outstanding performance in polarization-dependent amplitude (or intensity) manipulation of optical waves, making them a popular choice for creating high-resolution grayscale and colorful images.

#### ***Polarization-selective phase manipulation***

A variety of phase control mechanisms can be employed to design anisotropic nanostructures for optical phase manipulation, resulting in high-degree-of-freedom optical wavefront shaping. Here, we provide a brief overview of representative works that utilize various phase control mechanisms and discuss the design strategies for nanostructures to achieve polarization-selective phase manipulation. A more detailed discussion about how metasurfaces manipulate optical phase can be found in recent review articles [118, 119]. The phase of optical waves can be completely controlled through nanostructures by adjusting the complex coefficients in their transmission and reflection matrices. This is initially achieved by modulating the phase delay caused by optical resonances within the nanostructures. As shown in Fig. 5(a), a V-shaped nanostructure supporting both "symmetric" and "antisymmetric" resonance modes has been proposed to realize full control of the optical wavefront [120]. The V-shaped nanostructure consists of two arms of equal length connected at one end. By changing the lengths of the two arms and the included angle between them, the amplitude and phase of the cross-polarized transmission coefficient  $T_{yx}$  can be well manipulated. Eight V-shaped nanostructures with varying structural parameters and orientation angles, whose cross-polarized transmission coefficients  $T_{yx}$  have identical amplitude but different phase delays, are designed to realize full control of the wavefront of cross-polarized outgoing waves, as illustrated in Fig. 5(b). This approach, based on resonance phase, has two main drawbacks: low efficiency and a narrow operational waveband. The former is due to the metallic thin planar design, while the latter is caused by the dispersion and the finite wavelength range of optical resonances. The efficiency of optical phase manipulation can be significantly improved by using few-layer or lossless dielectric nanostructures [121–129]. Meanwhile, broadband optical phase manipulation can be achieved through the expansion of resonance band width and the utilization of geometric phase. Geometric phase can be easily implemented by nanostructures with spatially modulated orientation angles [118]. For nanostructures with nonzero circularly cross-polarized coefficients, the circularly polarized transmitted or reflected waves with opposite helicity to the incident waves exhibit an additional phase delay of  $\pm 2\theta$  (where  $\pm$  correspond to the helicity of incident wave and  $\theta$  represents the orientation angle of the nanostructure). Therefore, a phase shift can be tuned from 0 to  $2\pi$  for the outgoing waves with opposite helicity as the nanostructures are rotated from 0 to  $\pi$ , enabling full control of the optical wavefront of outgoing waves with opposite helicity, as illustrated in Fig. 5(c) [130]. The propagation phase, resulting from the propagation of optical waves within nanostructures, has

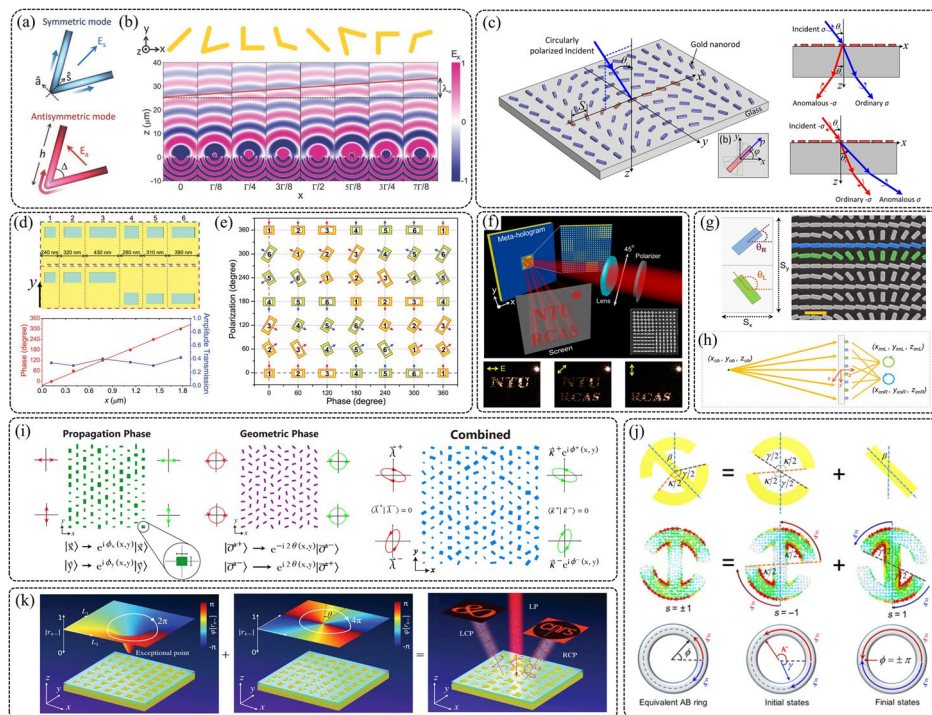


**Fig. 5** Polarization-selective phase manipulation based on anisotropic nanostructures. **a** Schematic of resonant modes in V-shaped plasmonic nanostructures. **b** Optical wavefront manipulation based on V-shaped nanostructure. **c** Schematic illustration of a dipole antenna array for achieving polarization-dependent phase manipulation under circularly-polarized incidence. **d** Bilayer nano-apertures with varying structural parameters and lateral displacement between the layers, and the transmission phase and amplitude of them under  $y$ -polarized incidence. **e** Complete control over the phase and polarization of transmitted waves through the six nanostructures with varying orientation angles. **f** Schematic illustration of polarization-selective meta-holography based on anisotropic plasmonic nanostructures and the experimentally measured hologram. **g** The building block of chiral lens and a SEM image of the fabricated chiral lens. **h** Imaging principle of the chiral lens. **i** Conceptual schematic for achieving independent phase control of arbitrary orthogonal states of polarization. **j** Schematic of a metasurface platform designed to break the symmetric restriction of the geometric phase. **k** Combination of exceptional topological phase and geometric phase to realize independent manipulation of LCP and RCP waves. **a, b** adapted from Ref. [120], Copyright 2011, with permission from American Association for the Advancement of Science. **c** adapted from Ref. [130], Copyright 2012, with permission from American Chemical Society. **d, e** adapted from Ref. [131], Copyright 2015, with permission from Wiley–VCH Verlag GmbH & Co. KGaA, Weinheim. **f** adapted from Ref. [134], Copyright 2014, with permission from American Chemical Society. **g, h** adapted from Ref. [136], Copyright 2016, with permission from American Chemical Society. **i** adapted from Ref. [54], Copyright 2017, with permission from American Physical Society. **j** adapted from Ref. [139], Copyright 2019, with permission from American Physical Society. **k** adapted from Ref. [143], Copyright 2021, with permission from American Association for the Advancement of Science

also been extensively utilized for optical phase manipulation [131, 132]. For example, anisotropic bilayer nanostructures, composed of pairs of nanoapertures, can serve as metal–insulator–metal waveguides [132]. By changing the structural parameters and lateral translation between the nanoapertures in the bilayer, as illustrated in Fig. 5(d), these structures exhibit comparable transmittance and a phase increment of  $\pi/3$  covering the entire  $2\pi$  range. Importantly, the transmitted waves are linear-polarized waves with their polarization direction aligned along the short axis of the nanoaperture. The polarization direction of transmitted waves can be easily manipulated by changing the orientation angle of the nanoaperture pairs. This approach enables the simultaneous manipulation

of polarization state and phase of transmitted waves, as demonstrated in Fig. 5(e), facilitating the generation of vector beams with arbitrary spatial variation of phase and linear polarization [133].

Based on the mechanism of phase modulation discussed above, anisotropic nanostructures have been further utilized to achieve polarization-selective optical phase manipulation. A reflective-type plasmonic metasurface composed of cross nanoantennas has been shown to be a promising option for the realization of polarization-controlled dual meta-holograms with high contrast, as illustrated in Fig. 5(f) [134]. In this approach, a set of 16 different cross nanoantennas with distinct resonance phase were designed to realize 4-bit phase encoding for two orthogonal linear polarization states. The cross-shaped nanostructures are designed as a combination of two nanorods, and their optical resonances in the two orthogonal polarization directions can be independently adjusted by changing the length of the nanorods, resulting in the independent phase manipulation in two orthogonal linear polarization channels. Compare to resonance phase, the geometric phase has been widely used to manipulate the phase of cross-polarized outgoing waves under circularly polarized incidence [135–138]. However, the geometric phase has the phase conjugation limitation, which prevents the independent phase manipulation of LCP and RCP waves. To overcome this challenge, a metasurface can incorporate two anisotropic nanostructures in a single unit cell to manipulate the phase of cross-polarized waves under LCP and RCP incidence respectively. As illustrated in Fig. 5(g) and (h), a metasurface whose unit cell composed of two nanofins acting as half-wave plates was proposed to realize polarization-selective light focusing [136]. The two nanofins are designed to implement the two required phase profiles to focus incident LCP and RCP waves, respectively. Other methods for achieving this include realizing the required phase profiles in different spatial regions or encoding the required phase profiles into one [137, 138]. However, these approaches result in unwanted interference between the LCP and RCP channels. With the combination of propagation phase and geometric phase, anisotropic nanostructures have been demonstrated as a potent platform for independent phase manipulation of arbitrary orthogonal states of polarization, as shown in Fig. 5(i) [54]. This method greatly enhances the capacity of anisotropic nanostructures for polarization-selective optical wavefront manipulation. Furthermore, an anisotropic metallic nanostructure composed of a pair of arcs with varying radii and a half-wave plate (shown in Fig. 5(j)) has been demonstrated as another effective approach for realizing spin-symmetry breaking geometric phase [139–142]. This nanostructure mimics the single ballistic Aharonov-Bohm ring. When the spin waves interact with the meta-atoms and experience a cyclic evolution, light can acquire a geometric phase shift akin to the Aharonov-Anandan phase observed in fermion particles. Through the combination of the Aharonov-Anandan and geometric phase, the symmetric restriction of the geometric phase is broken. Lately, the topological features of non-Hermitian matrices operating near their singular points (exceptional points) has been exploited to realize optical phase engineering [143–147]. As shown in Fig. 5(k), spin-selective optical wavefront manipulation can be realized by combining the robust topological phase around the exceptional point and the geometric phase. These advanced developments demonstrate the great potential of metasurfaces composed of anisotropic nanostructures for achieving polarization-selective and -multiplexed wavefront manipulation.

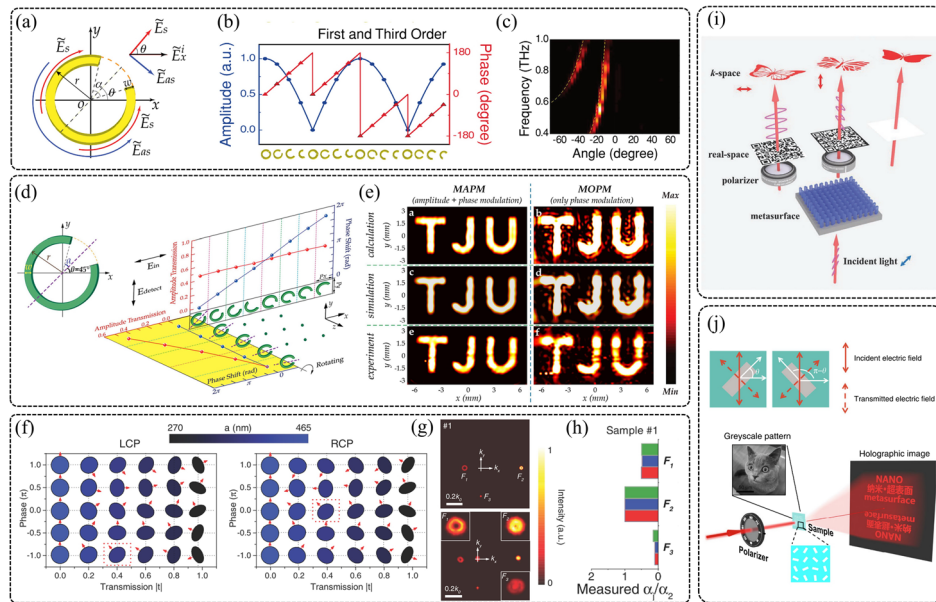


**Fig. 6** Polarization-selective complex amplitude manipulation based on anisotropic nanostructures. **a** Schematic of C-shaped antenna with symmetric and anti-symmetric resonant modes. **b** Amplitude and phase profiles of a metasurfaces designed with four C-shaped antennas for generating two diffraction orders. **c** Measured diffraction of the metasurface. **d** Realizing complex amplitude manipulation based on C-shape split-ring resonators. **e** Numerically calculated, simulated, and experimentally measured hologram generated by phase-modulated metasurfaces and complex amplitude-modulated metasurfaces respectively. **f** Dielectric nanopillars for the realization of complex amplitude manipulation of LCP and RCP incidence respectively. **g** Theoretical and measured intensity distributions of three optical functionalities in  $k$ -space implemented by using a complex amplitude-modulated metasurface, in which  $|F_1\rangle$ ,  $|F_2\rangle$ ,  $|F_3\rangle$  are designed as vortex light with order of 3, 1, 0, respectively. **h** The designed, calculated, and measured energies of each functionality. **i** Schematic illustration of a dielectric metasurface that can encode a QR code in real space and a vectorial holographic image in  $k$ -space. **j** Upper panel: schematic of one intensity to two phases mapping based on Malus' law. Lower panel: Reconstructing a greyscale image in the near field and a Fourier holographic image in the far field simultaneously through intensity and phase manipulation with nanobrick. **a**, **b**, **c** adapted from Ref. [148], Copyright 2014, with permission from Wiley–VCH Verlag GmbH & Co. KGaA, Weinheim. **d**, **e** adapted from Ref. [149], Copyright 2016, with permission from Springer Nature, under a Creative Commons Attribution 4.0 International License. **f**, **g**, **h** adapted from Ref. [150], Copyright 2019, with permission from Wiley–VCH Verlag GmbH & Co. KGaA, Weinheim. **i** adapted from Ref. [151], Copyright 2021, with permission from Wiley–VCH Verlag GmbH & Co. KGaA, Weinheim. **j** adapted from Ref. [152], Copyright 2020, with permission from Springer Nature, under a Creative Commons Attribution 4.0 International License

### Polarization-dependent complex amplitude manipulation

Up to this point, we have discussed representative works utilizing anisotropic nanostructures for polarization-selective manipulation of the amplitude or phase of optical waves. However, achieving complete control over the propagation of optical waves requires simultaneous manipulation of both amplitude and phase, which is crucial for wavefront shaping, holography and optical encryption [148–155]. A metasurface composed of C-shaped nanoantennas with different structural parameters has been proposed to realize the complete control over the complex amplitude of cross-polarized optical waves under  $x$ -polarized incidence [148]. As shown in Fig. 6(a), the designed C-shaped nanoantenna have anisotropic optical resonances. Both the symmetric and anti-symmetric resonance modes are excited simultaneously under  $x$ -polarized incidence, resulting in a  $y$ -polarized outgoing wave. The amplitude and phase of the  $y$ -polarized outgoing



wave can be easily manipulated by changing the structural parameters of the C-shaped nanoantenna and its orientation angle  $\theta$ . Metasurfaces composed of orderly arranging C-shaped nanoantennas in space have been utilized to realize meta-gratings with controllable diffraction orders. Figures 6(b) and (c) present an example of a meta-grating featuring two diffraction orders. The C-shaped nanoantenna has also been used to realize meta-holography with reduced noise and high resolution [149]. As illustrated in Fig. 6(d), the C-shaped nanoantenna can be used to realize independent manipulation of phase and amplitude of cross-polarized waves under linearly polarized incidence. As a result, the holographic image quality can be significantly improved, as shown in Fig. 6(e). The ability to manipulate the complex amplitude of optical waves is also advantageous in designing multifunctional metadevices. A design strategy based on the momentum analysis method has been proposed to manipulate the full Fourier components of the optical field, resulting in optical multifunction integration with eliminated noise and a customizable energy configuration [150]. Manipulating the full Fourier components of the optical field based on this design strategy necessitates simultaneous control over both amplitude and phase of optical waves. The efficacy of this design strategy has been confirmed through employment of dielectric nanopillars. The dielectric nanopillars can manipulate the complex amplitude of cross-polarized transmitted waves under LCP or RCP incidence by adjusting their structural parameters and orientation angles, as illustrated in Fig. 6(f). Figure 6(g) and (h) demonstrate the successful integration of three optical functionalities in  $k$ -space with a customized energy ratio using a designed metasurface composed of these dielectric nanopillars. Meanwhile, the manipulation of complex amplitude of optical waves based on anisotropic nanostructures allows for polarization-selective control of the optical field in both near and far field. For instance, a dielectric metasurface composed of nanorods has been proposed to simultaneously encode grayscale images in real-space and holographic images in  $k$ -space, as illustrated in Fig. 6(i) [151]. The complex amplitude of transmitted waves with orthogonal linear polarization states can be well modulated by adjusting the structural parameters and orientation angle of nanorods. The encoded grayscale images can only be observed by selecting the correct polarization component of the transmitted wave with an analyzer. The phase profiles of different polarization components are used to reconstruct the distinct holographic images in  $k$ -space. For another example, a Malus metasurface composed of aluminum nanorods has been demonstrated as a good candidate for independent manipulation of both the amplitude and phase of optical waves [152]. Due to the one intensity to two phases mapping based on Malus' law, it can realize a high-resolution continuous grayscale pattern at the sample surface and a multistep phase-only holographic image in far field, as illustrated in Fig. 6(j). These works demonstrate the significant practical value of anisotropic nanostructures for optical field manipulation.

#### ***Polarization manipulation in multiple domains***

The representative approaches discussed in Section "Optical polarization manipulation" focused on effectively manipulating the polarization state of optical waves. Recent advances in anisotropic nanostructures further validate their effectiveness for manipulating the distribution of polarization states in both spatial and momentum domains. Metasurfaces composed of anisotropic nanostructures have been demonstrated as

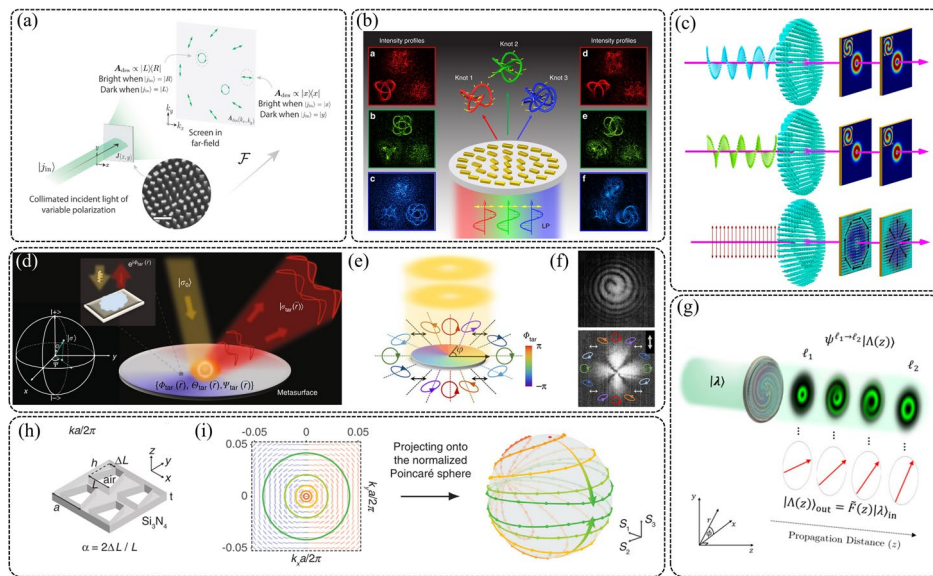


**Fig. 7** Polarization manipulation in multiple domains. **a** Schematic illustration of a polarization-analyzing hologram. **b** Generation of color-selective 3D polarization structures based on a metasurface consisting of gold nanorods. The measured intensity profiles of 3D polarization structures at three different operational wavelengths under illumination of linearly polarized incidence before (Left plane) and after (right plane) passing through an analyzer. **c** Schematic of an all-dielectric metasurface for the generation of longitudinally varying vector vortex beams. **d** Generation of arbitrary vectorial optical fields based on metasurfaces exhibiting full-matrix yet inhomogeneous Jones-matrix distributions. **e** Schematic of a designed meta-device to generate a vortex beam with varying ellipticity. **f** Interference pattern between the transmitted vortex beam and a spherical wave, and the recorded image for the generated vortex beam after passing through a linear polarizer. **g** Schematic of a versatile total angular momentum plate for simultaneous control of the polarization state and orbital angular momentum along the optical path. **h** A schematic of the anisotropic nanostructure and the definition of the asymmetry parameter  $\alpha$ . **i** The circular loops of polarization states mapped from the Brillouin zone to the Poincaré sphere. **a** adapted from Ref. [156], Copyright 2021, with permission from American Association for the Advancement of Science. **b** adapted from Ref. [159], Copyright 2022, with permission from Springer Nature, under a Creative Commons Attribution 4.0 International License. **c** adapted from Ref. [160], Copyright 2022, with permission from Wiley-VCH Verlag GmbH & Co. KGaA, Weinheim. **d, e, f** adapted from Ref. [161], Copyright 2021, with permission from Springer Nature, under a Creative Commons Attribution 4.0 International License. **g** adapted from Ref. [163], Copyright 2021, with permission from Springer Nature, under a Creative Commons Attribution 4.0 International License. **h, i** adapted from Ref. [164], Copyright 2017, with permission from American Physical Society

powerful platforms for achieving independent complex amplitude manipulation of optical waves with orthogonal polarization states at the subwavelength scale. Due to the fact that any polarization state can be decomposed into two orthogonal polarization vectors, such as LCP and RCP, metasurfaces have showcased their immense potential for spatial manipulation of polarization states. For example, a recent approach has validated that optical far-field distribution with customizable polarization response can be achieved by modulating multiple coefficients in the transmission or reflection matrices of anisotropic nanostructures. As shown in Fig. 7(a), a far-field with a polarization-dependent response described by  $\mathbf{A}(k_x, k_y)$  can be implemented by anisotropic nanostructures with customizable Jones matrix transfer function  $\mathbf{J}(x, y)$  [156]. It demonstrates that the spatial distribution of the polarization state in the far field can be easily modulated by designing nanostructures with desired Jones matrices. A more straightforward approach for spatial manipulation of polarization state involves the control of complex amplitude

of the orthogonal polarized beams [157–160]. Figure 7(b) illustrates the realization of color-selective three-dimensional (3D) polarization structures based on a planar metallic metasurface composed of anisotropic nanorods [159]. The metasurface is designed as a multi-foci metalens in 3D space to focus both LCP and RCP light beams while controlling their phase difference. The phase of far-field LCP and RCP radiation is modulated by controlling the geometric phase via adjusting the orientation angle of nanorods. Similarly, by integrating long-focal-depth vortex beams with different focal lengths into LCP and RCP states, as well as their superposition, longitudinally varying vector vortex beams have been realized via an all-dielectric metasurface by modulating both the propagation and geometric phases (shown in Fig. 7(c)) [160]. Moreover, precise control over the Jones matrix  $J(x, y)$  of metasurfaces enables intricate manipulation of polarization states, providing a powerful platform for generation of vector and vortex beams. For instance, vectorial optical field with arbitrarily designed wavefronts and polarization distributions has been realized with metasurface, as shown in Fig. 7(d) to (f) [161]. Importantly, by designing the Jones matrix of every unit cell in the metasurface, the metasurface can exhibit an inhomogeneous Jones matrix, providing control capabilities for both the local spin and global wavefront of optical waves. A novel approach using metasurfaces allows for arbitrary polarization control along the propagation direction, regardless of incident polarization [162]. This is achieved by transforming the incident waveform into pencil-like beams with different polarizations, altering polarization locally as light travels. Furthermore, such approach has been used to realize a versatile total angular momentum plate for simultaneous control of the polarization state and orbital angular momentum along the optical path, as shown in Fig. 7(g) [163]. The polarization state distribution can be manipulated not only in real 3D space but also in momentum space by using metasurfaces. In addition to controlling the angular dispersion of nanostructures, as discussed above, recent analysis on the topological nature of optical bound states in the continuum (BICs) provides a new degree of freedom for polarization manipulation in momentum space [164–167]. For instance, a planar photonic crystal slab (as shown in Fig. 7(h)) has been proposed to control the polarization states of far-field radiations with varying  $k$  vectors [164]. By adjusting the asymmetric structural parameter  $\alpha$ , the in-plane inversion  $C_2$  symmetry of the photonic crystal slab is disrupted, resulting in the elimination of the at- $\Gamma$  BICs (vortex polarization singularities in momentum space, V point) and the arising of pairs of two opposing chirality C points, shown in Fig. 7(i). The continuous variation and complete coverage on the Poincare sphere can be achieved by manipulating the polarization state along circular loops with different radii. Precise manipulation of the V and C points in momentum space enables effective control over the polarization state of far-field radiation.

#### ***Polarization-selective manipulation of nonlinear waves***

The developments discussed above demonstrate the significant importance and unparalleled potential for utilizing anisotropic nanostructures in polarization-dependent optical field manipulation. It should be noted that, through the concept of nonlinear geometric phase and the selection rules for harmonic generation of circular-polarized fundamental waves, both isotropic and anisotropic nanostructures have been widely utilized for achieving polarization-selective manipulation of intensity and phase of nonlinear

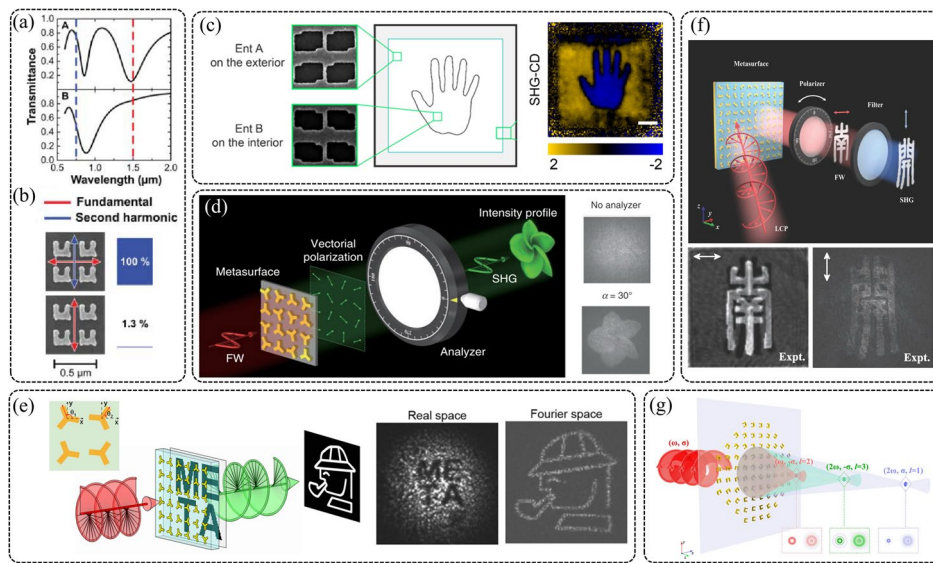


**Fig. 8** Polarization-selective manipulation of nonlinear waves. **a** Measured linear-optical spectrum of a periodic array composed of split-ring resonators under (upper) horizontal and (lower) vertical polarized incidence. **b** The polarization state of the SHG emission and the normalized SHG signal strengths. **c** Schematic of a hand pattern whose exterior and interior regions are formed by a pair of enantiomeric chiral mirrors, and its SHG-CD image. **d** Generating of a polarization profile of the SHG wave by using a nonlinear metasurface for optical encryption, and the experimental captured images with and without a linear analyzer. **e** Real and Fourier space image encoding based on a nonlinear metasurface, and the measured real and Fourier space images at SH frequency. **f** Linear and nonlinear information encryption based on a Malus metasurface. **g** Linear and nonlinear spin- and wavelength-selective generation of focusing optical vortices via a nonlinear metasurface. **a, b** adapted from Ref. [180], Copyright 2006, with permission from American Association for the Advancement of Science. **c** adapted from Ref. [181], Copyright 2017, with permission from American Chemical Society. **d** adapted from Ref. [182], Copyright 2018, with permission from American Physical Society. **e** adapted from Ref. [183], Copyright 2020, with permission from American Chemical Society. **f** adapted from Ref. [184], Copyright 2024, with permission from Wiley-VCH Verlag GmbH & Co. KGaA, Weinheim. **g** adapted from Ref. [168], Copyright 2018, with permission from Wiley-VCH Verlag GmbH & Co. KGaA, Weinheim

harmonics, thereby enabling nonlinear wavefront manipulation with high degree of freedom [168–179]. Anisotropic nanostructures were originally used to enhance second harmonic generation (SHG). For example, the magnetic-dipole resonances in the split-ring resonators have been used to realize polarization-selective enhancement of SHG, as shown in Fig. 8(a) and (b) [180]. For horizontal incidence, the magnetic-dipole resonances can be excited, leading to a 500-fold enhancement of SHG above the noise level, with its polarization angle predominantly vertical. Conversely, when exciting the split-ring resonators with vertically polarized incidence, only a small signal just above the noise level can be observed. Spin-selective enhancement of SHG has also been reported. As illustrated in Fig. 8(c), a pair of enantiomeric chiral mirrors have been proposed to realize spin-selective enhancement of SHG [181]. Due to the controllable polarization state of SHG with nanostructures, they have been further used to manipulate the spatial distribution of the polarization profile of the SHG. The nonlinear photonic metasurface depicted in Fig. 8(d) consists of meta-atoms exhibiting threefold rotational ( $C_3$ ) symmetry, enabling the realization of a vectorial polarization profile for nonlinear imaging [182]. The polarization angle of the SHG wave is locally controlled by the in-plane rotation of nonlinear meta-atoms, denoted as  $\theta(x, y)$ . Moreover, such design has also been proved as an effective approach for nonlinear multidimensional optical information

encoding. The nonlinear metasurface, illustrated in Fig. 8(e), demonstrates its capacity for realizing both real and Fourier space image encoding [183]. Each unit cell of this metasurface is comprised of two meta-atoms featuring unique orientation angles. This configuration enables control over both the amplitude and phase of the SHG by modulating the interference between SHG signals originating from these two meta-atoms, achieved through adjustments to their respective orientation angles. In addition to the polarization-selective manipulation of nonlinear harmonics, anisotropic nanostructures have been utilized to achieve the simultaneous manipulation of both linear and nonlinear waves. A nonlinear Malus metasurface has been proposed to realize linear and nonlinear information encryption, as shown in Fig. 8(f) [184]. The polarization angle of both linear and nonlinear waves can be manipulated by adjusting the orientation angle of the U-shaped resonators. This capability allows for the simultaneous encoding of intensity for both fundamental and harmonic waves. Such U-shaped resonators has also been proved as good candidate for achieving spin-selective simultaneous manipulation of the wavefronts of both fundamental and harmonic waves, as shown in Fig. 8(g) [168, 169]. The anisotropic nanostructures exhibit remarkable capabilities not only in polarization-selective optical field manipulation but also in polarization-selective nonlinear optical field manipulation.

#### Optical polarization state measurement based on anisotropic nanostructures

Due to the unprecedented capability of anisotropic nanostructures in polarization-selective intensity and phase manipulation of optical waves, they have found extensive applications in achieving integration and minimization of polarimetry [40]. It has demonstrated that anisotropic nanostructures allow for a complete measurement of the Stokes vector  $\mathbf{S} = [S_0, S_1, S_2, S_3]$  by measuring the intensities of different polarization components of light. The elements in the matrix  $\mathbf{S}$  are defined as  $S_0 = I$ ,  $S_1 = I_x - I_y$ ,  $S_2 = I_{45} - I_{-45}$ ,  $S_3 = I_R - I_L$ , where  $I$  represents the total intensity of light, and  $I_x$ ,  $I_y$ ,  $I_{45}$  and  $I_{-45}$  are the intensity of light in linear polarization bases along the  $x$ ,  $y$ ,  $45^\circ$  and  $-45^\circ$  directions, respectively.  $I_R$  and  $I_L$  are the intensities of the RCP and LCP light. A conventional setup for measuring the Stokes vector is shown in the upper plane of Fig. 9(a). It consists of a waveplate (either half or quarter), a Wollaston prism and a lens that focuses the beams onto photodetectors. The four elements of the Stokes vector can be determined based on the detected signals obtained under three distinct conditions: without any waveplate, with a half-wave plate, and with a quarter-waveplate. The functionalities of these three optical components in conventional setup can be integrated and implemented by using dielectric metasurfaces composed of anisotropic nanostructure. For example, Fig. 9(b) shows a unit cell of a dielectric metasurfaces consisting of  $2 \times 3$  sub arrays, enabling the complete determination of all elements of the Stokes vector [185]. The sub arrays are composed of dielectric birefringent nanostructures that can realize independent phase manipulation of two orthogonal polarization states. These six arrays are specifically designed to function as distinct metalenses, with each row's two arrays capable of focusing a particular pair of orthogonal polarization states ( $x/y$ ,  $\pm 45^\circ$ , LCP/RCP) to two different focal points. The Stokes vector then can be obtained by measuring the intensities of the six focus points for each unit cell and take the average. Recent approaches have further demonstrated that these sub-arrays can be designed as

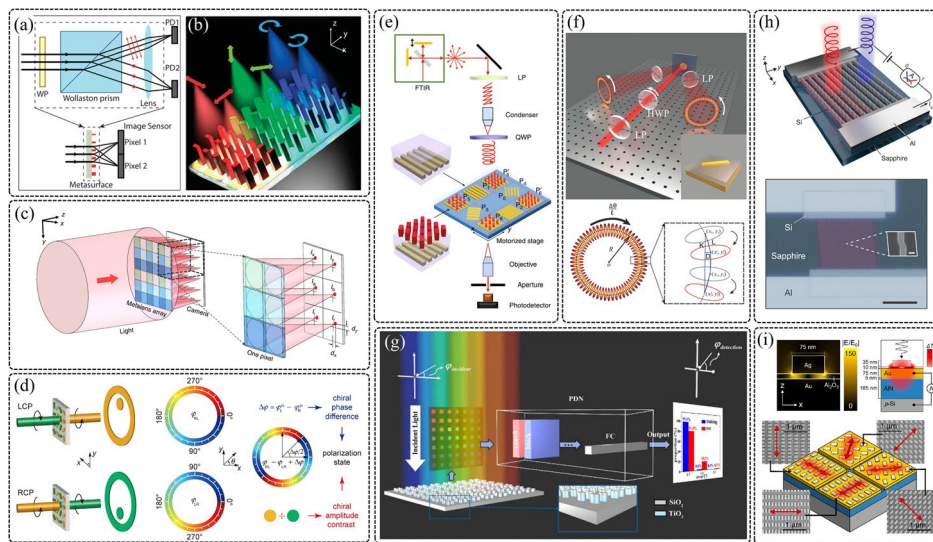


**Fig. 9** Optical polarization state measurement based on anisotropic nanostructures. **a** Schematic of a conventional setup and a compact metasurface used for polarimetry. **b** Schematic of a dielectric metasurface designed for spatially selective focusing of different polarizations. **c** Schematic of a dielectric metalens system for measuring spatial polarization profile. **d** Concept and working mechanism of holographic polarimetry based on metasurface. **e** Schematic of an on-chip array of polarization filters designed to fully characterize the polarization state of the incident wave. **f** Schematic of a high-order vector beam generated using a metasurface for highly sensitive polarization rotation measurement. **g** Schematic of colorimetric polarization-angle detection based on asymmetrical all-dielectric metasurfaces. **h** Schematic of a circular dichroism photodetector using dislocated high-index semiconductor metasurfaces and its reflected optical micrograph. **i** Upper panel: Simulated resonance-induced electric field enhancement within the nanogap cavity at 740 nm and schematic of heat generation within the nanogap cavity. Lower panel: Schematic and SEM images of four photodetectors optimized for absorption of light polarized at the angle of the red arrows. **a, b** adapted from Ref. [185], Copyright 2018, with permission from American Chemical Society. **c** adapted from Ref. [186], Copyright 2018, with permission from Springer Nature, under a Creative Commons Attribution 4.0 International License. **d** adapted from Ref. [188], Copyright 2019, with permission from Optical Society of America. **e** adapted from Ref. [189], Copyright 2019, with permission from Springer Nature, under a Creative Commons Attribution 4.0 International License. **f** adapted from Ref. [191], Copyright 2020, with permission from Wiley-VCH Verlag GmbH & Co. KGaA, Weinheim. **g** adapted from Ref. [192], Copyright 2022, with permission from Optical Society of America. **h** adapted from Ref. [195], Copyright 2023, with permission from Optical Society of America. **i** adapted from Ref. [196], Copyright 2023, with permission from American Chemical Society

crosstalk-free broadband achromatic metalenses, capable of direct and accurate measurement without calibration, significantly enhancing the device's practicality [36]. Since that each unit cell enables the measurement of Stokes vector at the corresponding spatial position, the designed metasurface has been further used to realize polarimetric imaging. Furthermore, a similar design (as shown in Fig. 9(c)) has been utilized for polarimetric beam profiling [186]. In this design, the spatial distribution of polarization state is obtained based on the measured intensities of the six focus points of each unit cell, while the phase gradient profile is retrieved by measuring the displacements of the focus points in the  $x$  and  $y$  directions. The limited spatial resolution caused by the large period of the unit cell remains one of the primary challenges that need to be addressed in order to advance this kind of design. Another advanced method for complete measurement of the Stokes vector based on polarization-selective light wavefront manipulation with anisotropic nanostructure [43, 187]. For instance, a recent approach demonstrated that matrix Fourier optics enables the design of the orders of diffraction gratings composed

of anisotropic nanostructures as polarizers for an arbitrarily selected set of polarization states [187]. With this method, a two-dimensional diffraction grating has been successfully used for the realization of full-Stokes polarimeter and polarization imagery by measuring four projective polarization states in parallel. Since that optical waves with arbitrary polarization states can be decomposed into two orthogonal polarization components, the polarization state of light can also be obtained by measuring the intensity of the two orthogonal polarization components and their phase difference. Based on this principle, a polarization-dependent holography has been proposed to realize direct polarization detection in a single measurement [188]. As illustrated in Fig. 9(d), an interleaved plasmonic metasurface designed based on geometric phase can generate two holograms with mirror symmetry under LCP and RCP illumination. The two holograms are partially overlapped with a spatially varying phase difference. The amplitude of the LCP and RCP components of the incident light and the phase difference between them can be read from the holographic images. More specifically, the amplitude contrast of LCP and RCP components can be obtained based on the holographic images of the disks, while the phase difference between them can be resolved based on the intensity distribution of the holographic image of the overlapped ring. Note that the Stokes vector can also be obtained based on this method. This approach with a good level of accuracy provides a novel candidate for polarization measurement.

The above-mentioned approaches for optical polarization state measurement are based on polarization-selective light wavefront manipulation with anisotropic nanostructures. Anisotropic nanostructures functioning as polarization filters can also be used to realize full-Stokes polarimetric measurement [189, 190]. For instance, six polarization filters, including four linear polarization filters ( $P_1$  to  $P_4$ ) and two circular polarization filters ( $P_5$  and  $P_6$ ), are integrated into one chip for full measurement of the Stokes vector, as shown in Fig. 9(e) [189]. Here, the  $P'_5$  and  $P'_6$  are backup structures for  $P_5$  and  $P_6$ , which can be used to identify the Stokes vector at a different operational wavelength. The linear polarization filters are nanowire gratings with orientation angles of 0, 45, -45 and 90 degrees (with respect to the  $x$ -axis). The two kind of circular polarization filters are selectively transmitting only LCP and RCP waves, respectively. The six filters are used to measure the intensities of six polarization components of incident light, while an empty area in the center of the chip is used to measure the total light intensity. Then, the full elements of Stokes vector can be calculated. This design holds significant potential for facilitating chip-integrated polarimeters.

Undoubtedly, there is a high demand on novel methodologies employing anisotropic nanostructures to accurately and rapidly measure light polarization. In addition to direct measurement of light polarization, indirect measurement of light polarization based on anisotropic nanostructures has been also widely investigated. As shown in Fig. 9(f), polarization rotation measurement with a dynamic range of 180 degrees and a sensitivity of about 0.01 has been realized based on a high-order vector beam generated by a plasmonic metasurface composed of nanorods [191]. The proposed metasurface is designed to generate two vector beams under linearly polarized incidence, which are the superposition of two vortex beams carrying opposite spins as well as orbital angular momentum. The vector beam forms a lobed fringe pattern when passed through a linear polarizer. The rotation angle of the incident

linearly polarized wave can be determined by observing the rotation of these lobes with a camera. This approach offers a new route toward the development of compact high-precision polarimeters. As another example, quantitative colorimetric polarization-angle detection has been achieved by using asymmetrical all-dielectric nanostructures and a deep-learning network, as illustrated in Fig. 9(g) [192]. An arrayed color palette composed of asymmetric nanopillars with high-performance polarization-sensitive structural colors has been used to generate different color distributions under linearly polarized illumination with different polarization angles. The deep-learning network is trained to identify the polarization angle of the linearly polarized incident light based on the color distribution of the color palette. This method can accurately detect extremely slight variations in polarization angle within approximately 1 s, provides a new paradigm for polarization detection. A recent approach also demonstrated that combining a metasurface array composed of nanostructures with weak anisotropic responses and a deep-learning network enables the development of a single-shot full-Stokes polarization camera [193]. Previous approaches for polarization state manipulation typically involve anisotropic nanostructures with a high polarization extinction ratio [189, 190] or arrays of anisotropic nanostructures with polarization-selective functionalities [36, 185, 186], leading to a complex design and optimization process and a limited operational bandwidth. By leveraging deep-learning networks and other reconstruction methods, metasurface arrays composed of nanostructures with randomly designed structural parameters, considered as random polarization sensing matrices, have been demonstrated as effective candidates to overcome these limitations, achieving high-accuracy polarization measurement and imaging.

Recently, photodetector for light polarization measurement has drawn great attention due to the integration and ease of use of the device [194–198]. For example, a dielectric metasurface, which displays a guided-mode resonance only for a circular polarization of interest, has been employed to build an integrated photodetector for circularly polarized light detection, as shown in Fig. 9(h) [195]. The circular dichroism of the designed metasurface reach the theoretical maximum, resulting in a resonantly enhanced external quantum efficiency for RCP light over LCP light. As a result, the circular polarization states can be directly distinguished. As another example, integrated polarization-sensing metasurface composed of anisotropic nanorods (as illustrated in Fig. 9(i)) has been proposed to realize ultrathin pyroelectric photodetector, which can measure the angle of linear polarization of arbitrary incident polarized light with high-sensitivity, high-speed, and high-accuracy [196]. In this design, the nanostructures act as polarization-sensitive antennas that can efficiently absorb light with specific linear polarization state at their resonant wavelength. The absorbed waves are converted to heat that propagates downward and is exploited by the underlying pyroelectric photodetector. The anisotropic nanostructures with high polarization sensitivity play a pivotal role in the realization of these high-performance photodetectors for light polarization detection and will continue to exert significant influence.



### **Polarization-multiplexed optical wave manipulation based on few-layer and polyatomic metasurfaces composed of anisotropic nanostructures**

In the preceding discussion, we mainly focus on nanostructures with simple structural configurations, such as nanorods, elliptic nanocylinders, L-shaped and C-shaped nano-antennas. Despite the significant progress made by these anisotropic nanostructures in polarization-dependent optical wave manipulation and polarization detection, their efficiency and flexibility are limited due to a restricted degree of design freedom. Recent advancements indicate that anisotropic nanostructures with few-layer or polyatomic configurations provide greater design flexibility, enabling highly efficient polarization-multiplexed optical wave manipulation, expanding the number of polarization channels, and facilitating novel functionalities. In this section, we highlighting their impressive versatility and efficacy for polarization-multiplexed optical wave manipulation.

#### ***Polarization-multiplexed optical wave manipulation based on few-layer metasurfaces***

Compared to planar metasurfaces with simple structural configurations, few-layer nanostructures have four key advantages for optical wave manipulation: first, the abundant interlayer light-matter interactions within few-layer nanostructures enable not only the excitation of electric dipole but also that of magnetic dipole and higher-order multipoles, resulting in highly efficient optical field manipulation [199–201]. For example, a tri-layer metasurface exhibiting both electric and magnetic responses have been proposed to realize photonic spin hall effect with a measured efficiency of approximately 91%, as illustrated in Fig. 10(a) to (c) [201]. The anisotropic tri-layer nanostructures that construct the metasurface can efficiently convert circularly polarized incident waves into transmitted waves with orthogonal polarization states. On this basis, the wavefront of the transmitted wave is easily modulated by using geometric phase. Second, different optical functionalities realized by planar metasurfaces can be integrated in a few-layer design, greatly enhancing the flexibility of artificial nanostructures for optical wave manipulation, and enabling a suite of new functionalities that may not be achievable with planar metasurfaces [202–205]. As illustrated in Fig. 10(d), an all-dielectric metasurface consisting of two planar metasurfaces on either side of a quartz substrate has been proposed to realize the integration of different optical functionalities [204]. For TM incidence, the first metasurface is designed to minimize the spot size and the second metasurface is designed to control the beam deflection angle. As a result, this metasurface functioning as a doublet lens for TM-polarized incidence. Third, the structural mirror symmetry with respect to the plane perpendicular to the wave propagation direction cannot be broken in planar nanostructures, while the structural symmetry of few-layer nanostructures can be arbitrarily designed [44, 51]. This characteristic enables the few-layer metasurfaces to achieve some optical functions that planar nanostructure cannot achieve. For instance, the asymmetric transmission of linearly polarized waves [206–208]. For planar nanostructures, their cross-polarized transmission coefficients  $T_{xy}$  and  $T_{yx}$  are always equal. Due to the reciprocity theorem, the relationship between their cross-polarized transmission coefficients under forward and backward incidences can be expressed as follows:  $T_{xy}^f = -T_{yx}^b$  and  $T_{yx}^f = -T_{xy}^b$  [206]. Taking  $x$ -polarized incidence as an example, the difference in transmittance between forward and backward incidences can be obtained as  $\Delta I_t = |T_{yx}^f|^2 - |T_{xy}^f|^2$ . Asymmetric transmission can be achieved

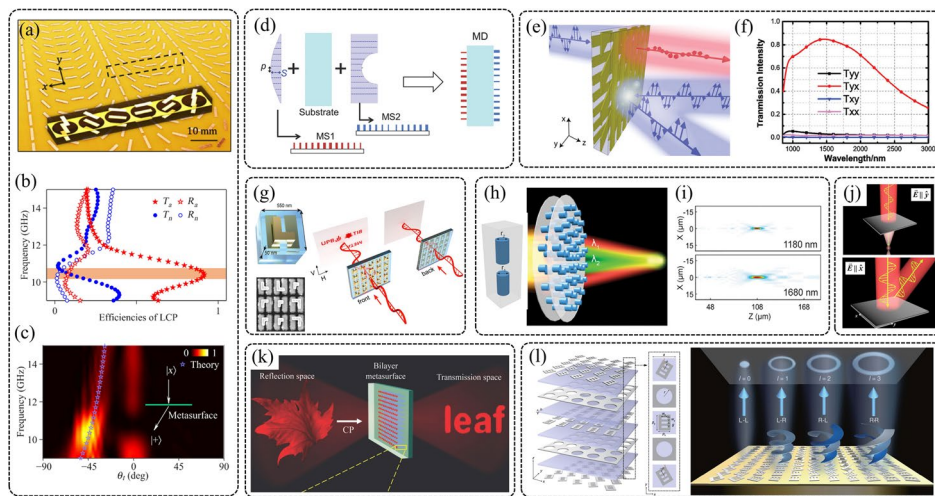


**Fig. 10** Polarization-selective and -multiplexed optical manipulation based on few-layer anisotropic nanostructures. **a** Picture of a fabricated tri-layer metasurface. **b** Absolute efficiencies of the four modes (normal and anomalous transmission and reflection waves) versus frequency for the tri-layer metasurface. **c** Measured intensities of transmission fields versus the frequency. **d** Schematic of an all-dielectric metasurface doublet. **e** Schematic of asymmetric transmission based on a tri-layer metasurfaces. **f** Simulated transmission intensity through the metasurface. **g** Left panel: Schematic of a bilayer nanostructure for nonreciprocal holography and the SEM image of a fabricated sample. Right panel: Schematic illustration of the polarization-dependent nonreciprocal hologram. **h** Schematic of a metasurface doublet focusing two wavelengths at the same focal distance, and its unit cell. **i** Simulated axial intensity distribution. **j** Schematic of a polarization multiplexed full-space bifunctional meta-device composed of four-layer nanostructures. **k** A conceptual diagram of full-space meta-holography based on a bilayer dielectric metasurface. **l** Schematic of the complete phase-modulation in quadruplex polarization channels based on a five-layer metasurfaces. **a**, **b**, **c** adapted from Ref. [201], Copyright 2017, with permission from American Physical Society. **d** adapted from Ref. [204], Copyright 2020, with permission from Wiley–VCH Verlag GmbH & Co. KGaA, Weinheim. **e**, **f** adapted from Ref. [208], Copyright 2016, with permission from Wiley–VCH Verlag GmbH & Co. KGaA, Weinheim. **g** adapted from Ref. [210], Copyright 2019, with permission from American Chemical Society. **h**, **i** adapted from Ref. [211], Copyright 2018, with permission from American Chemical Society. **j** adapted from Ref. [221], Copyright 2017, with permission from American Physical Society. **k** adapted from Ref. [222], Copyright 2022, with permission from Wiley–VCH Verlag GmbH & Co. KGaA, Weinheim. **l** adapted from Ref. [223], Copyright 2020, with permission from Springer Nature, under a Creative Commons Attribution 4.0 International License

when the two cross-polarized coefficients are not equal. If the co-polarized coefficient and one of the cross-polarized coefficients equal zero, diodelike asymmetric transmission can be realized [207]. The transmission coefficients of few-layer nanostructures can be independently manipulated by breaking the structural mirror symmetry, resulting in asymmetric transmission of linearly polarized waves with high efficiency. For example, a few-layer metasurface composed of coupled metallic sheets has been proposed to realize diodelike asymmetric transmission with broad bandwidth (FWHM bandwidth of  $1.7 \mu\text{m}$ ), robust angular tolerance, and high efficiency (80%), as shown in Fig. 10(e) and (f) [208]. Due to this feature, few-layer metasurfaces emerged as a powerful platform for the realization of polarization-selective asymmetric optical field manipulation [45, 209, 210]. For instance, a bilayer metasurface has been proposed to realize nonreciprocal polarization encryption of holographic images, as illustrated in Fig. 10(g) [210]. The unit cell of the bilayer metasurface consists of an L-shaped nanoantenna and two nanorods in combination. This bilayer nanostructures can realize the asymmetric transmission of linear-polarized waves [207], while the phase of transmitted cross-polarized waves can be manipulated by changing the structural parameters of the L-shaped

nanoantennas. With this design, the encoded holographic image can be observed in a particular linear cross-polarization channel, which disappears in the reverse propagation direction. Fourth, few-layer metasurfaces offer greater design flexibility, allowing for tailored transmission and reflection matrices. Specially, when the interlayer coupling is negligible, the transmission matrices of the few-layer metasurfaces can be seen as the product of each layer's matrices. Figure 10(h) and (i) show a metalens doublet whose unit cell consists of two nanocylinders with different diameters [211]. The overall phase and transmittance are calculated as the sum of the phase delay and product of the transmittance from each layer, enabling independent manipulation of light focusing at two distinct wavelengths. Besides this approach, few-layer metasurfaces have been extensively employed for wavelength- and polarization-selective optical field manipulation [212–214]. Due to these four key advantages, few-layer metasurfaces with tailored transmission and reflection matrices provides a fertile ground for polarization-multiplexed optical field manipulation [215–223]. For example, few-layer metasurfaces with customized transmission and reflection coefficients has been utilized to realize optical wave manipulation in the full space. As depicted in Fig. 10(j), a single device can now integrate beam-bending and focusing functionalities in a polarization-selective manner by simultaneously modulating the reflection coefficient  $R_{xx}$  and transmission coefficient  $T_{yy}$  [221]. Independent phase manipulation of cross-polarized transmitted and reflected waves under circularly polarized incidence has also been realized based on a dielectric bilayer metasurface, enabling full-space meta-holography [222]. As shown in Fig. 10(k), the reflection and transmission spaces display two distinct and independently designed holographic images. The polarization channels can be further expanded by independently modulating all the coefficients in the transmission and reflection matrices. A few-layer chirality-assisted metasurfaces, for which the phase of all four reflection coefficients can be independently manipulated, has been utilized to realize independent phase modulation for quadruplex polarization channels, as illustrated in Fig. 10(l) [223]. All these developments indicate that few-layer metasurfaces with customizable transmission and reflection matrices play increasingly important roles in polarization-multiplexed full-space optical field manipulation.

#### ***Polarization-multiplexed optical wave manipulation based on polyatomic metasurfaces***

Although few-layer metasurfaces offer significant advantages for polarization-multiplexed optical wave manipulation, their fabrication process is more complex compared to planar metasurfaces and requires higher precision in nanofabrication technology. Another way to increase the design flexibility of metasurfaces is by using multiple nanostructures within a single unit cell, which are referred to as polyatomic nanostructures. In traditional planar metasurfaces, where the unit cell is composed of only one nanostructure, the limited structural parameters restrict the ability to achieve arbitrary spatially varying scattering matrices. In contrast, when near-neighbor interactions are negligible, the transmission and reflection matrices of polyatomic nanostructures can be expressed as the sum of those of each individual nanostructure. This approach provides a viable alternative for attaining desired transmission and reflection coefficients, enabling polarization-selective optical wave manipulation with enhanced flexibility. Polyatomic metasurface have shown remarkable capacities for optical polarization manipulation and

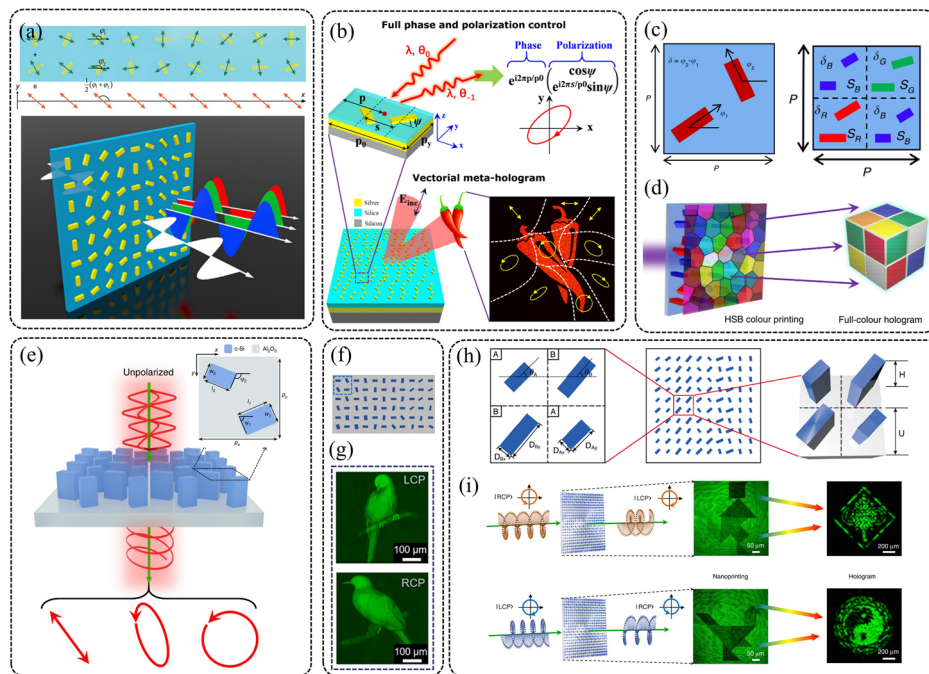


**Fig. 11** Multidimensional optical wave manipulation based on anisotropic polyatomic nanostructures. **a** Upper panel: schematic of a diatomic metasurface whose unit cell consists of two nanorods aligned in the same column. Lower panel: Schematic diagram illustrating the simultaneous manipulation of polarization and wavefront. **b** Illustration of a diatomic metasurface composed of two orthogonal plasmonic nanorods for full manipulation of the phase and polarization of the diffracted beam, and the realization of vectorial meta-holography. **c** Schematic of the unit cell and the super unit cell of a dielectric metasurface for spin-selective optical phase and intensity manipulation. **d** Schematic illustration of the integration of a colour printing and a full-colour hologram based on the dielectric metasurface. **e** Schematic of a diatomic metasurface that can directly operate with unpolarized incident light and generate arbitrary polarization states. **f** Schematic of a polyatomic metasurface for independent amplitude control of arbitrary orthogonal states of polarization. **g** Experimentally captured optical images of the polyatomic metasurface nanoprinting. **h** Schematic of a polyatomic metasurface, and **i** experimental validation of the integration of two nanoprinting images near the metasurface and two hologram images in the far field based on the polyatomic metasurface. **a** adapted from Ref. [224], Copyright 2017, with permission from American Chemical Society. **b** adapted from Ref. [225], Copyright 2018, with permission from American Chemical Society. **c, d** adapted from Ref. [230], Copyright 2019, with permission from Springer Nature, under a Creative Commons Attribution 4.0 International License. **e** adapted from Ref. [231], Copyright 2021, with permission from Springer Nature, under a Creative Commons Attribution 4.0 International License. **f, g** adapted from Ref. [232], Copyright 2020, with permission from American Physical Society. **h, i** adapted from Ref. [233], Copyright 2021, with permission from Springer Nature, under a Creative Commons Attribution 4.0 International License

polarization-multiplexed optical field manipulation [224–238]. For example, plasmonic diatomic metasurfaces whose unit cell consisting of two nanorods has been proposed to realize broadband half-wave plate, as shown in Fig. 11(a) [224]. The two nanorods in each unit cell function as linear polarizers. The phase of the cross-polarized transmitted waves from the two nanorods under circularly polarized incidence can be well manipulated by modulating the orientation angles  $\phi_1$  and  $\phi_2$  of the nanorods respectively. The combination of the two nanorods in one unit cell results in a broadband half-wave plate with optical axis at  $(\phi_1 + \phi_2)/2$ . Linear-polarized transmitted waves with polarization angle of  $\phi_1 + \phi_2 - \phi$  can be generated under a linearly polarized incidence with the polarization angle of  $\phi$ . Meanwhile, the transmission intensity of the polarization-converted transmitted waves is direct proportion to the square of  $\cos(\phi_1 - \phi_2)$ , which can

be modulated by changing the orientation angles  $\phi_1$  and  $\phi_2$ . Therefore, the wavefront of polarization-converted transmitted waves can be manipulated based on spatial intensity manipulation. By modulating the value of orientation angles  $\phi_1$  and  $\phi_2$  of the nanorods, both the polarization direction and the propagation direction of polarization-converted transmitted waves can be easily manipulated. This method demonstrates the potential of polyatomic metasurfaces for multidimensional optical wave manipulation. Plasmonic diatomic metasurfaces formed by two orthogonal nanorods has been further proposed and applied to realize vectorial holography, as illustrated in Fig. 11(b) [225]. By using displacement-targeted phase, the phase and polarization state of the negative first diffraction order can be manipulated by changing the global displacement from the unit cell boundary to the centroid of the two nanorods, the local displacement between the two nanorods and the orientation angle of the nanorods, resulting in high-fidelity and efficient vectorial holography. This approach offers a straightforward analytical framework for designing diatomic nanostructures, with a simple linear relationship between the structural parameters and the modulated phase/polarization parameters. Besides plasmonic polyatomic metasurfaces, dielectric polyatomic metasurfaces with high efficiency have been widely proposed for optical polarization manipulation and polarization-multiplexed optical wave manipulation [230–237]. For instance, a dielectric metasurface has been proposed for simultaneous and independent manipulation of the intensity and phase of cross-polarized transmitted waves at a single operational waveband under circularly polarized incidence. Its unit cell is composed of two c-silicon nanoblocks with different orientation angles  $\phi_1$  and  $\phi_2$  (as shown in Fig. 11(c)), and the intensity and phase of the cross-polarized transmitted waves under circular polarization are decided by the difference and sum of  $\phi_1$  and  $\phi_2$  respectively [230]. By incorporating diatomic nanostructures with different operational wavebands into a single unit cell, the metasurface can manipulate the complex amplitude of cross-polarized transmitted waves at three distinct wavebands (red, green, and blue light), enabling the integration of HSB colour printing and full-color meta-holography, as illustrated in Fig. 11(d). This approach facilitates the manipulation of optical fields in both near and far fields. Dielectric diatomic metasurfaces composed of two nanoblocks with different orientation angles and structural parameters in each unit cell have further been proposed to achieve all-in-one full Poincaré sphere polarizers, as shown in Fig. 11(e) [231]. By independently design the transmission matrices of the two nanoblocks, these polarizers enable selective transmission and conversion of a specific polarization state located at any position on the Poincaré sphere to its handedness-flipped state, while completely blocking its orthogonal state. In theory, this method demonstrates perfect dichroism of nearly 100%, and experimentally achieves over 90% for arbitrary polarization states. Moreover, the polyatomic metasurfaces exhibit significant advantages in the implementation of polarization-multiplexed optical field manipulation. For example, a dielectric metasurface whose unit cell composed of four rectangular nanopillars has been proposed to impose two arbitrary and independent amplitude profiles on a pair of orthogonal polarizations, as shown in Fig. 11(f) and (g) [232]. In this design, each unit cell is constructed using two types of nanopillars with distinct structural parameters and orientation angles. The diagonal nanopillars within the unit cell are identical in structure. The transmission coefficients of the nanopillars can be adjusted by modifying their structural parameters and orientation

angles. The transmitted waves from different nanopillars are collective interference with each other, and the transmission matrix of the unit cell is simply the sum of those of each individual nanopillar. With the greater design flexibility, the transmission coefficients of the unit cell can be arbitrarily tailored, resulting in independent amplitude manipulation of optical waves with orthogonal polarization states. It has been demonstrated that such polyatomic design can be used to realize simultaneous and independent manipulation of complex amplitude for orthogonal polarization states, enabling four-channel nano-printing hologram (Fig. 11(h) and (i)) [233]. By incorporating additional nanostructures within each unit cell, the design flexibility of the polyatomic metasurface is significantly enhanced. This provides great advantages for arbitrary optical polarization manipulation and enables polarization-multiplexed optical field manipulation.

### **Conclusion and outlook**

In summary, we have reviewed the representative developments and latest advances in anisotropic nanostructures for optical polarization manipulation, detection, and polarization-selective optical wave manipulation. We have summarized the design strategies for metasurfaces composed of anisotropic nanostructures and discussed the advantages of anisotropic nanostructures for optical polarization manipulation and polarization-selective optical wave manipulation. Additionally, we reviewed the representative methods for measuring optical polarization state based on anisotropic nanostructures. Moreover, we conducted a comprehensive analysis of recent advancements in few-layer and polyatomic metasurfaces composed of anisotropic nanostructures to showcase their remarkable versatility and efficacy in polarization-multiplexed optical wave manipulation. We believe that few-layer and polyatomic metasurfaces composed of anisotropic nanostructures will increasingly play a crucial role in polarization-multiplexed optical wave manipulation due to their exceptional design flexibilities. Here, we propose several promising directions in this research field that may further expand the range of applications for anisotropic nanostructures:

#### **Polarization manipulation in multiple domains**

Metasurfaces have recently demonstrated great potential for realizing optical polarization elements with novel functionalities through manipulation of optical polarization at multiple frequencies, in the momentum space, and at different locations along the wave propagating direction [161, 162, 239–242]. Further advancement in this research direction will facilitate the complete manipulation of optical waves across multiple domains.

#### **Nonorthogonal polarization-multiplexed manipulation of optical waves**

By adjusting the diagonal and off-diagonal coefficients in the transmission or reflection matrices, anisotropic metasurfaces can enable polarization multiplexing with two orthogonal polarization channels or even four polarization channels consisting of both co- and cross-polarized waves with orthogonal polarization states [22, 50, 223]. These methods achieve the theoretical maximum capacity of polarization multiplexing, which is limited by the dimension constraints of the transmission and reflection matrices. Recent advances indicate that anisotropic metasurfaces can also be used to realize

arbitrary nonorthogonal polarization multiplexing [243, 244]. Specially, by introducing the engineered noise to the precise solution of transmission matrix elements, a new approach utilizing polyatomic metasurfaces has been demonstrated as a powerful candidate to significantly expand the number of channels for polarization multiplexing [51]. These novel approaches are inspiring and may warrant further exploration in the fields of optical communication and encryption. Design strategies allowing a greater number of channels for polarization multiplexing remain highly desirable.

#### **Full-space complete manipulation of optical waves**

The coefficients of transmission and reflection matrices for few-layer metasurfaces can be independently adjusted. By incorporating multiple nanostructures into each layer of their unit cells, the degree of design flexibility for few-layer metasurfaces can be further enhanced [245, 246]. Such few-layer polyatomic metasurfaces hold great potential in achieving full-space polarization multiplexing, but new design and optimization methods are necessary due to the significantly increased structural parameters.

#### **Integrated devices for light emission and detection**

Anisotropic nanostructures with polarization control functionalities have demonstrated remarkable capabilities in manipulating light, making them invaluable in a wide range of integrated optical devices. These structures offer versatile means for both emitting and detecting light across various applications. For example, chiral dielectric nanostructures have been utilized to realize enhanced chiral emission [247, 248]. Moreover, anisotropic nanostructures have been employed for optical spectrum measurement [190, 249]. When integrated with compact cameras, complex polarization imaging can be implemented [193, 250]. Recent advancements in guided wave-driven metasurfaces further substantiate the immense potential of anisotropic nanostructures for on-chip polarization-multiplexed optical field manipulation [251–257].

#### **Devices with special scattering functionalities**

Since the transmission and reflection matrices of metasurfaces can be tailored, they are ideal candidates for realizing metadevices with spatial scattering functionalities that cannot be achieved using traditional optical materials. For example, circular dichroism with near 100% efficiency has been realized with a dielectric few-layer polyatomic metasurface [258]. Solid Poincaré sphere polarizer that can filter unpolarized incident light to light with any prescribed state of polarization and degree of polarization has been implemented based on dielectric metasurfaces [93]. A Poincaré sphere trajectory encoding approach based on metasurfaces has been reported [259]. This approach leverages a generalized form of Malus' law, governing universal 2D projections between arbitrary elliptical polarization pairs spanning the entire Poincaré sphere, enabling arbitrary polarization-selective intensity encodings.

#### **Abbreviations**

PCR	Polarization conversion rate
RCP	Right-handed circular polarization

LCP	Left-handed circular polarization
MIM	Metal–insulator–metal
FOV	Field of view
TE	Transverse electric
TM	Transverse magnetic
2D	Two-dimensional
3D	Three-dimensional
BICs	Bound states in the continuum
SHG	Second harmonic generation
FWHM	Full width at half maximum
QR	Quick Response

#### Authors' contributions

Methodology, ZL, and SC; writing—original draft preparation, ZL, WL and YZ; writing—review and editing, ZL, WL, YZ, HC, SZ and SC; supervision, SC. All authors read and approved the final manuscript.

#### Funding

This work was supported by the National Key Research and Development Program of China (Nos. 2021YFA1400601 and 2022YFA1404501), the National Natural Science Fund for Distinguished Young Scholars (No. 11925403), the New Cornerstone Science Foundation, the National Natural Science Foundation of China (Nos. 12122406, 12192253, U22A20258, 12274237 and 12274239).

#### Availability of data and materials

Data sharing is not applicable to this article as no new datasets were created in this review.

#### Declarations

##### Competing interests

The authors declare that they have no competing interests.

Received: 17 July 2024 Revised: 11 September 2024 Accepted: 21 September 2024

Published online: 03 October 2024

#### References

- Singh D. Fundamentals of Optics. 2nd ed. New Delhi: Prentice Hall India Pvt. Ltd; 2015. p. 452–518.
- He C, He H, Chang J, Chen B, Ma H, Booth MJ. Polarisation optics for biomedical and clinical applications: a review. *Light Sci Appl*. 2021;10:194.
- Yoon G, Tanaka T, Zentgraf T, Rho J. Recent progress on metasurfaces: applications and fabrication. *J Phys D Appl Phys*. 2021;54: 383002.
- Leitis A, Tseng ML, John-Herpin A, Kivshar YS, Altug H. Wafer-Scale Functional Metasurfaces for Mid-Infrared Photonics and Biosensing. *Adv Mater*. 2021;33:2102232.
- Geng G, Zhu W, Pan R, Zhang Z, Gu C, Li J. Precise tailoring of multiple nanostructures based on atomic layer assembly via versatile soft-templates. *Nano Today*. 2021;38: 101145.
- Pan R, Li Z, Liu Z, Zhu W, Zhu L, Li Y, Chen S, Gu C, Li J. Rapid bending origami in micro/nanoscale toward a versatile 3D metasurface. *Laser Photonics Rev*. 2020;14:1900179.
- Su VC, Chu CH, Sun G, Tsai DP. Advances in optical metasurfaces: fabrication and applications. *Opt Express*. 2018;26:13148–82.
- Chen S, Li Z, Liu W, Cheng H, Tian J. From single-dimensional to multidimensional manipulation of optical waves with metasurfaces. *Adv Mater*. 2019;31:1802458.
- Dorrah AH, Capasso F. Tunable structured light with flat optics. *Science*. 2022;376:eabi6860.
- Neshev D, Aharonovich I. Optical metasurfaces: new generation building blocks for multi-functional optics. *Light Sci Appl*. 2018;7:58.
- Luo X. Subwavelength artificial structures: opening a new era for engineering optics. *Adv Mater*. 2019;31:1804680.
- Chen HT, Taylor AJ, Yu N. A review of metasurfaces: physics and applications. *Rep Prog Phys*. 2016;79: 076401.
- Hsiao HH, Chu CH, Tsai DP. Fundamentals and applications of metasurfaces. *Small Methods*. 2017;1:1600064.
- Kamali SM, Arbabi E, Arbabi A, Faraon A. A review of dielectric optical metasurfaces for wavefront control. *Nanophotonics*. 2018;7:1041–68.
- Koshelev K, Kivshar Y. Dielectric resonant metaphotonics. *ACS Photonics*. 2020;8:102–12.
- Yu N, Capasso F. Flat optics with designer metasurfaces. *Nat Mater*. 2014;13:139–50.
- Pors A, Nielsen MG, Della Valle G, Willatzen M, Albrektsen O, Bozhevolnyi SI. Plasmonic metamaterial wave retarders in reflection by orthogonally oriented detuned electrical dipoles. *Opt Lett*. 2011;36:1626–8.
- Ding F, Wang Z, He S, Shalae VM, Kildishev AV. Broadband high-efficiency half-wave plate: a supercell-based plasmonic metasurface approach. *ACS Nano*. 2015;9:4111–9.
- Yu N, Aieta F, Genevet P, Kats MA, Gaburro Z, Capasso F. A broadband, background-free quarter-wave plate based on plasmonic metasurfaces. *Nano Lett*. 2012;12:6328–33.
- Khan MI, Tahir FA. A compact half and quarter-wave plate based on bi-layer anisotropic metasurface. *J Phys D Appl Phys*. 2017;50:43LT04.



21. Ma Z, Hanham M, Gong Y, Hong M. All-dielectric reflective half-wave plate metasurface based on the anisotropic excitation of electric and magnetic dipole resonances. *Opt Lett*. 2018;43:911–4.
22. Chen Y, Gao J, Yang X. Direction-controlled bifunctional metasurface polarizers. *Laser Photonics Rev*. 2018;12:1800198.
23. Kurosawa H, Choi B, Sugimoto Y, Iwanaga M. High-performance metasurface polarizers with extinction ratios exceeding 12000. *Opt Express*. 2017;25:4446–55.
24. Jiang SC, Xiong X, Hu YS, Hu YH, Ma GB, Peng RW, Sun C, Wang M. Controlling the polarization state of light with a dispersion-free metastructure. *Phys Rev X*. 2014;4: 021026.
25. Zhao Y, Alù A. Tailoring the dispersion of plasmonic nanorods to realize broadband optical meta-waveplates. *Nano Lett*. 2013;13:1086–91.
26. Li Z, Liu W, Cheng H, Chen S, Tian J. Realizing broadband and invertible linear-to-circular polarization converter with ultrathin single-layer metasurface. *Sci Rep*. 2015;5:18106.
27. Huang CP, Zhang Y, Wang YL, Kong LB. Arbitrarily directional and tunable polarization rotating effect with coupled metal screens. *Phys Rev Appl*. 2018;10: 064038.
28. Li Z, Liu W, Cheng H, Chen S, Tian J. Spin-selective transmission and devisable chirality in two-layer metasurfaces. *Sci Rep*. 2017;7:8204.
29. Chen S, Liu W, Li Z, Cheng H, Tian J. Metasurface-empowered optical multiplexing and multifunction. *Adv Mater*. 2020;32:1805912.
30. Dong F, Chu W. Multichannel-independent information encoding with optical metasurfaces. *Adv Mater*. 2019;31:1804921.
31. Deng ZL, Wang ZQ, Li FJ, Hu MX, Li X. Multi-freedom metasurface empowered vectorial holography. *Nanophotonics*. 2022;11:1725–39.
32. Zhang Z, Wen D, Zhang C, Chen M, Wang W, Chen S, Chen X. Multifunctional light sword metasurface lens. *ACS Photonics*. 2018;5:1794–9.
33. Zhao H, Zhang C, Guo J, Liu S, Chen X, Zhang Y. Metasurface hologram for multi-image hiding and seeking. *Phys Rev Appl*. 2019;12: 054011.
34. Badloe T, Seong J, Rho J. Trichannel spin-selective metalenses. *Nano Lett*. 2023;2:6958–65.
35. Kang H, Kim H, Kim K, Rho J. Printable Spin-Multiplexed Metasurfaces for Ultraviolet Holographic Displays. *ACS Nano*. 2024;18:21504–11.
36. Zhang Y, Pu M, Jin J, Lu X, Guo Y, Cai J, Zhang F, Ha Y, He Q, Xu M, Li X, Ma X, Luo X. Crosstalk-free achromatic full Stokes imaging polarimetry metasurface enabled by polarization-dependent phase optimization. *Opto-Electron Adv*. 2022;5:220058–61.
37. Yang F, Lin HI, Shalaginov MY, Stoll K, An S, Rivero-Baleine C, Kang M, Agarwal A, Richardson K, Zhang H, Hu J, Gu T. Reconfigurable parfocal zoom metalens. *Adv Opt Mater*. 2022;10:2200721.
38. Yang F, Lin HI, Chen P, Hu J, Gu T. Monocular depth sensing using metalens. *Nanophotonics*. 2023;12:2987–96.
39. Pors A, Nielsen MG, Bozhevolnyi SI. Plasmonic metagratings for simultaneous determination of Stokes parameters. *Optica*. 2015;2:716–23.
40. Intaravanne Y, Chen X. Recent advances in optical metasurfaces for polarization detection and engineered polarization profiles. *Nanophotonics*. 2020;9:1003–14.
41. Bai J, Yao Y. Highly efficient anisotropic chiral plasmonic metamaterials for polarization conversion and detection. *ACS Nano*. 2021;15:14263–74.
42. Wang R, Han J, Liu J, Tian H, Sun W, Li L, Chen X. Multi-foci metalens for terahertz polarization detection. *Opt Lett*. 2020;45:3506–9.
43. Shah YD, Dada AC, Grant JP, Cumming DR, Altuzarra C, Nowack TS, Lyons A, Clerici M, Faccio D. An all-dielectric metasurface polarimeter. *ACS Photonics*. 2022;9:3245–52.
44. Li Z, Liu W, Cheng H, Chen S. Few-layer metasurfaces with arbitrary scattering properties. *Sci China Phys Mech*. 2020;63: 284202.
45. Chen K, Ding G, Hu G, Jin Z, Zhao J, Feng Y, Jiang T, Alù A, Qiu CW. Directional janus metasurface. *Adv Mater*. 2020;32:1906352.
46. Liu W, Li Z, Ansari MA, Cheng H, Tian J, Chen X, Chen S. Design strategies and applications of dimensional optical field manipulation based on metasurfaces. *Adv Mater*. 2023;35:2208884.
47. Yu S, Cheng J, Li Z, Liu W, Cheng H, Tian J, Chen S. Electromagnetic wave manipulation based on few-layer metasurfaces and polyatomic metasurfaces. *ChemPhysMater*. 2022;1:6.
48. Kim I, Jang J, Kim G, Lee J, Badloe T, Mun J, Rho J. Pixelated bifunctional metasurface-driven dynamic vectorial holographic color prints for photonic security platform. *Nat Commun*. 2021;12:3614.
49. Guo X, Zhong J, Li B, Qi S, Li Y, Li P, Wen D, Liu S, Wei B, Zhao J. Full-color holographic display and encryption with full-polarization degree of freedom. *Adv Mater*. 2022;34:2103192.
50. Bao Y, Nan F, Yan J, Yang X, Qiu CW, Li B. Observation of full-parameter Jones matrix in bilayer metasurface. *Nat Commun*. 2022;13:7550.
51. Xiong B, Liu Y, Xu Y, Deng L, Chen CW, Wang JN, Peng R, Lai Y, Liu Y, Wang M. Breaking the limitation of polarization multiplexing in optical metasurfaces with engineered noise. *Science*. 2023;379:294–9.
52. Menzel C, Rockstuhl C, Lederer F. Advanced Jones calculus for the classification of periodic metamaterials. *Phys Rev A*. 2010;82: 053811.
53. Arbabi A, Horie Y, Bagheri M, Faraon A. Dielectric metasurfaces for complete control of phase and polarization with subwavelength spatial resolution and high transmission. *Nat Nanotech*. 2015;10:937–43.
54. Mueller JB, Rubin NA, Devlin RC, Groever B, Capasso F. Metasurface polarization optics: independent phase control of arbitrary orthogonal states of polarization. *Phys Rev Lett*. 2017;118: 113901.
55. Jing L, Wang Z, Yang Y, Shen L, Zheng B, Gao F, Wang H, Li E, Chen H. Diodelike spin-orbit interactions of light in chiral metasurfaces. *IEEE T Antenn Propag*. 2018;66:7148–55.
56. Rubin NA, D'Aversa G, Chevalier P, Shi Z, Chen WT, Capasso F. Matrix Fourier optics enables a compact full-Stokes polarization camera. *Science*. 2019;365:eaax1839.

57. Raeker BO, Grbic A. Compound metaoptics for amplitude and phase control of wave fronts. *Phys Rev Lett*. 2019;122: 113901.
58. Bao Y, Wen L, Chen Q, Qiu CW, Li B. Toward the capacity limit of 2D planar Jones matrix with a single-layer metasurface. *Sci Adv*. 2021;7:eabh0365.
59. Bao Y, Ni J, Qiu CW. A minimalist single-layer metasurface for arbitrary and full control of vector vortex beams. *Adv Mater*. 2019;32:1905659.
60. Li Z, Liu W, Ma D, Yu S, Cheng H, Choi DY, Tian J, Chen S. Inverse Design of Few-Layer Metasurfaces Empowered by the Matrix Theory of Multilayer Optics. *Phys Rev Appl*. 2022;17: 024008.
61. Ma W, Liu Z, Kudyshev ZA, Boltasseva A, Cai W, Liu Y. Deep learning for the design of photonic structures. *Nat Photonics*. 2021;15:77–90.
62. Liu Z, Zhu D, Rodrigues SP, Lee KT, Cai W. Generative model for the inverse design of metasurfaces. *Nano Lett*. 2018;18:6570–6.
63. Ma W, Cheng F, Liu Y. Deep-learning-enabled on-demand design of chiral metamaterials. *ACS Nano*. 2018;12:6326–34.
64. Zhu D, Liu Z, Raju L, Kim AS, Cai W. Building multifunctional metasystems via algorithmic construction. *ACS Nano*. 2021;15:2318–26.
65. Trisno J, Wang H, Wang HT, Ng RJ, Daqiqeh Rezaei S, Yang JK. Applying machine learning to the optics of dielectric nanoblobs. *Adv Photonics Res*. 2020;1:2000068.
66. Zhang Y, Cheng Y, Chen M, Xu R, Yuan L. Ultracompact metaimage display and encryption with a silver nanopolarizer based metasurface. *Appl Phys Lett*. 2020;117: 021105.
67. Dai Q, Zhou N, Deng L, Deng J, Li Z, Zheng G. Dual-channel binary gray-image display enabled with malus-assisted metasurfaces. *Phys Rev Appl*. 2020;14: 034002.
68. Deng Y, Cai Z, Ding Y, Bozhevolnyi SI, Ding F. Recent progress in metasurface-enabled optical waveplates. *Nanophotonics*. 2022;11:2219–44.
69. Liu Z, Li Z, Liu Z, Li J, Cheng H, Yu P, Liu W, Tang C, Gu C, Li J, Chen S, Tian J. High performance broadband circularly polarized beam deflector by mirror effect of multi-nanorod metasurfaces. *Adv Funct Mater*. 2015;25:5428.
70. Li Z, Liu W, Cheng H, Choi DY, Chen S, Tian J. Arbitrary manipulation of light intensity by bilayer aluminum metasurfaces. *Adv Opt Mater*. 2019;7:1900260.
71. Zang X, Liu S, Cheng Q, Xie J, Zhu Y, Wang Y. Lower-order-symmetry induced bandwidth-controllable terahertz polarization converter. *J Opt*. 2017;19: 115103.
72. Hu S, Yang S, Liu Z, Li J, Gu C. Broadband cross-polarization conversion by symmetry-breaking ultrathin metasurfaces. *Appl Phys Lett*. 2017;111: 241108.
73. Lin B, Wang B, Meng W, Da X, Li W, Fang Y, Zhu Z. Dual-band high-efficiency polarization converter using an anisotropic metasurface. *J Appl Phys*. 2016;119: 183103.
74. Xu J, Li R, Wang S, Han T. Ultra-broadband linear polarization converter based on anisotropic metasurface. *Opt Express*. 2018;26:26235–41.
75. Dong G, Shi H, Xia S, Zhang A, Xu Z, Wei X. Ultra-broadband perfect cross polarization conversion metasurface. *Opt Commun*. 2016;365:108–12.
76. Liu W, Chen S, Li Z, Cheng H, Yu P, Li J, Tian J. Realization of broadband cross-polarization conversion in transmission mode in the terahertz region using a single-layer metasurface. *Opt Lett*. 2015;40:3185.
77. Lévesque Q, Makhisiyan M, Bouchon P, Pardo F, Jaeck J, Bardou N, Dupuis C, Haidar R, Pelouard JL. Plasmonic planar antenna for wideband and efficient linear polarization conversion. *Appl Phys Lett*. 2014;104: 111105.
78. Huang CP. Efficient and broadband polarization conversion with the coupled metasurfaces. *Opt Express*. 2015;23:32015–24.
79. Grady NK, Heyes JE, Chowdhury DR, Zeng Y, Reiten MT, Azad AK, Taylor AJ, Dalvit DAR, Chen HT. Terahertz metamaterials for linear polarization conversion and anomalous refraction. *Science*. 2013;340:1304–7.
80. Zhao Y, Alù A. Manipulating light polarization with ultrathin plasmonic metasurfaces. *Phys Rev B*. 2011;84: 205428.
81. Yu P, Li J, Tang C, Cheng H, Liu Z, Li Z, Liu Z, Gu C, Li J, Chen S, Tian J. Controllable optical activity with non-chiral plasmonic metasurfaces. *Light Sci Appl*. 2016;5: e16096.
82. Arbabi A, Faraon A. Fundamental limits of ultrathin metasurfaces. *Sci Rep*. 2017;7:43722.
83. Nakata Y, Taira Y, Nakanishi T, Miyamaru F. Freestanding transparent terahertz half-wave plate using subwavelength cut-wire pairs. *Opt Express*. 2017;25:2107–14.
84. Kruk S, Hopkins B, Kravchenko II, Miroshnichenko A, Neshev DN, Kivshar YS. Broadband highly efficient dielectric metadevices for polarization control. *APL Photonics*. 2016;1: 030801.
85. Hu Y, Wang X, Luo X, Ou X, Li L, Chen Y, Yang P, Wang S, Duan H. All-dielectric metasurfaces for polarization manipulation: principles and emerging applications. *Nanophotonics*. 2020;9:3755–80.
86. Li Z, Liu W, Cheng H, Chen S, Tian J. Manipulation of the photonic spin Hall effect with high efficiency in gold-nanorod-based metasurfaces. *Adv Opt Mater*. 2017;5:1700413.
87. Cheng H, Chen S, Yu P, Li J, Deng L, Tian J. Mid-infrared tunable optical polarization converter composed of asymmetric graphene nanocrosses. *Opt Lett*. 2013;38:1567.
88. Li J, Yu P, Cheng H, Liu W, Li Z, Xie B, Chen S, Tian J. Optical polarization encoding using graphene-loaded plasmonic metasurfaces. *Adv Opt Mater*. 2016;4:91.
89. Yu P, Li J, Liu N. Electrically tunable optical metasurfaces for dynamic polarization conversion. *Nano Lett*. 2021;21:6690–5.
90. Qiu M, Jia M, Ma S, Sun S, He Q, Zhou L. Angular dispersions in terahertz metasurfaces: physics and applications. *Phys Rev Appl*. 2018;9: 054050.
91. Shi Z, Zhu AY, Li Z, Huang YW, Chen WT, Qiu CW, Capasso F. Continuous angle-tunable birefringence with freeform metasurfaces for arbitrary polarization conversion. *Sci Adv*. 2020;6:eaba3367.
92. Wang EW, Yu SJ, Phan T, Dhuey S, Fan JA. Arbitrary achromatic polarization control with reconfigurable metasurface systems. *Laser Photonics Rev*. 2023;17:2200926.

93. Wang S, Wen S, Deng ZL, Li X, Yang Y. Metasurface-Based Solid Poincaré Sphere Polarizer. *Phys Rev Lett.* 2023;130:123801.
94. Fu R, Chen K, Li Z, Yu S, Zheng G. Metasurface-based nanoprinting: principle, design and advances. *Opto-Electron Sci.* 2022;1: 220011.
95. Yue F, Zhang C, Zang XF, Wen D, Gerardot BD, Zhang S, Chen X. High-resolution grayscale image hidden in a laser beam. *Light Sci Appl.* 2018;7:17129.
96. Deng J, Li Z, Li J, Zhou Z, Gao F, Qiu C, Yan B. Metasurface-Assisted Optical Encryption Carrying Camouflaged Information. *Adv Opt Mater.* 2022;10:2200949.
97. Li Z, Ren R, Deng J, Deng L, Li G, Zheng G. Non-orthogonal-polarization multiplexed metasurfaces for tri-channel gray-imaging. *Opt Express.* 2021;29:134–44.
98. Wang Z, Cheng F, Winsor T, Liu Y. Optical chiral metamaterials: a review of the fundamentals, fabrication methods and applications. *Nanotechnology.* 2016;27: 412001.
99. Li Z, Liu W, Cheng H, Choi DY, Chen S, Tian J. Spin-selective full-dimensional manipulation of optical waves with chiral mirror. *Adv Mater.* 2020;32:1907983.
100. Cheng J, Li Z, Choi DY, Yu S, Liu W, Wang H, Zhang Y, Cheng H, Tian J, Chen S. Spin-selective full and subtle light intensity manipulation with diatomic metasurfaces. *Adv Opt Mater.* 2023;10:2202329.
101. Dai Q, Guan Z, Chang S, Deng L, Tao J, Li Z, Li Z, Yu S, Zheng G, Zhang S. A single-celled Tri-functional metasurface enabled with triple manipulations of light. *Adv Funct Mater.* 2020;30:2003990.
102. Cao Y, Tang L, Li J, Wang J, Dong ZG. Dual-wavelength complementary grayscale imaging by an ultrathin metasurface. *Opt Lett.* 2020;45:5181–4.
103. Proust J, Bedu F, Gallas B, Ozerov I, Bonod N. All-dielectric colored metasurfaces with silicon Mie resonators. *ACS Nano.* 2016;10:7761–7.
104. Li Z, Dai Q, Deng L, Zheng G, Li G. Structural-color nanoprinting with hidden watermarks. *Opt Lett.* 2021;46:480–3.
105. Dai Q, Zhu G, Zhang W, Li J, Li Z, Cui H, Wei K, He Z, Guan Z, Zheng G. Dual-channel anticounterfeiting color-nanoprinting with a single-size nanostructured metasurface. *Opt Express.* 2022;30:33574–87.
106. Kristensen A, Yang JK, Bozhevolnyi SI, Link S, Nordlander P, Halas NA, Mortensen NA. Plasmonic colour generation. *Nat Rev Mater.* 2016;2:1–14.
107. Zhang X, Cheng J, Yue W, Li Z, Choi DY, Li Y, Li H, Lee S, Chen S, Gao S. Twofold optical display and encryption of binary and grayscale images with a wavelength-multiplexed metasurface. *Nanophotonics.* 2023;12:3747–56.
108. Koirala J, Shrestha VR, Park CS, Lee SS, Choi DY. Polarization-controlled broad color palette based on an ultrathin one-dimensional resonant grating structure. *Sci Rep.* 2017;7:40073.
109. Kim M, Kim I, Jang J, Lee D, Nam KT, Rho J. Active color control in a metasurface by polarization rotation. *Appl Sci.* 2018;8:982.
110. Yang B, Liu W, Li Z, Cheng H, Chen S, Tian J. Polarization-sensitive structural colors with hue-and-saturation tuning based on all-dielectric nanopixels. *Adv Opt Mater.* 2018;6:1701009.
111. Ellenbogen T, Seo K, Crozier KB. Chromatic plasmonic polarizers for active visible color filtering and polarimetry. *Nano Lett.* 2012;12:1026–31.
112. Heydari E, Sperling JR, Neale SL, Clark AW. Plasmonic Color Filters as Dual-State Nanopixels for High-Density Micro-image Encoding. *Adv Funct Mater.* 2017;27:1701866.
113. Liu HL, Zhang B, Gao T, Wu X, Cui F, Xu W. 3D chiral color prints for anti-counterfeiting. *Nanoscale.* 2019;11:5506–11.
114. Wang L, Wang T, Yan R, Yue X, Wang H, Wang Y, Zhang J, Yuan X, Zeng J, Wang J. Color Printing and Encryption with Polarization-Switchable Structural Colors on All-Dielectric Metasurfaces. *Nano Lett.* 2023;23:5581–7.
115. Daqiqeh Rezaei S, Dong Z, Chan JYE, Trisno J, Ng RJH, Ruan Q, Qiu CW, Mortensen NA, Yang JK. Nanophotonic structural colors. *ACS Photonics.* 2020;8:18–33.
116. Zang X, Dong F, Yue F, Zhang C, Xu L, Song Z, Chen M, Chen PY, Buller GS, Zhu Y, Zhuang S, Chu W, Zhang S, Chen X. Polarization encoded color image embedded in a dielectric metasurface. *Adv Mater.* 2018;30:1707499.
117. Huo P, Song M, Zhu W, Zhang C, Chen L, Lezec HJ, Lu Y, Agrawal A, Xu T. Photorealistic full-color nanopainting enabled by a low-loss metasurface. *Optica.* 2020;7:1171–2.
118. Guo Y, Pu M, Zhang F, Xu M, Li X, Ma X, Luo X. Classical and generalized geometric phase in electromagnetic metasurfaces. *Photonics Insights.* 2022;1:R03.
119. Chen S, Li Z, Zhang Y, Cheng H, Tian J. Phase manipulation of electromagnetic waves with metasurfaces and its applications in nanophotonics. *Adv Opt Mater.* 2018;6:1800104.
120. Yu N, Genevet P, Kats MA, Aieta F, Tetti JP, Capasso F, Gaburro Z. Light propagation with phase discontinuities: generalized laws of reflection and refraction. *Science.* 2011;334:333–7.
121. Sun S, Yang KY, Wang CM, Juan TK, Chen WT, Liao CY, et al. High-efficiency broadband anomalous reflection by gradient meta-surfaces. *Nano Lett.* 2012;12:6223–9.
122. Qin F, Ding L, Zhang L, Monticone F, Chum CC, Deng J, et al. Hybrid bilayer plasmonic metasurface efficiently manipulates visible light. *Sci Adv.* 2016;2: e1501168.
123. Ding F, Chang B, Wei Q, Huang L, Guan X, Bozhevolnyi SI. Versatile polarization generation and manipulation using dielectric metasurfaces. *Laser & Photonics Rev.* 2020;14:200016.
124. Gao S, Park CS, Lee SS, Choi DY. A highly efficient bifunctional dielectric metasurface enabling polarization-tuned focusing and deflection for visible light. *Adv Opt Mater.* 2019;7:1801337.
125. Jiang ZH, Kang L, Yue T, Xu HX, Yang Y, Jin Z, et al. A single noninterleaved metasurface for high-capacity and flexible mode multiplexing of higher-order Poincaré sphere beams. *Adv Mater.* 2020;32:1903983.
126. Tang S, Cai T, Liang JG, Xiao Y, Zhang CW, Zhang Q, et al. High-efficiency transparent vortex beam generator based on ultrathin Pancharatnam-Berry metasurfaces. *Opt Express.* 2019;27:1816–24.
127. Zhu W, Fan Y, Yang R, Geng G, Fu Q, Gu C, et al. Polarization-Multiplexed Silicon Metasurfaces for Multi-Channel Visible Light Modulation. *Adv Funct Mater.* 2022;32:2200013.
128. Ma Z, Li Y, Li Y, Gong Y, Maier SA, Hong M. All-dielectric planar chiral metasurface with gradient geometric phase. *Opt Express.* 2018;26:6067–78.

129. Guo Z, Zhu L, Shen F, Zhou H, Gao R. Dielectric metasurface based high-efficiency polarization splitters. *RSC Adv.* 2017;7:9872–9.
130. Huang L, Chen X, Muhlenbernd H, Li G, Bai B, Tan Q, Jin G, Zentgraf T, Zhang S. Dispersionless phase discontinuities for controlling light propagation. *Nano Lett.* 2012;12:5750–5.
131. Khorasaninejad M, Capasso F. Broadband multifunctional efficient meta-gratings based on dielectric waveguide phase shifters. *Nano Lett.* 2015;15:6709–15.
132. Li J, Chen S, Yang H, Li J, Yu P, Cheng H, et al. Simultaneous control of light polarization and phase distributions using plasmonic metasurfaces. *Adv Funct Mater.* 2015;25:704.
133. Yu P, Chen S, Li J, Cheng H, Li Z, Liu W, et al. Generation of vector beams with arbitrary spatial variation of phase and linear polarization using plasmonic metasurfaces. *Opt Lett.* 2015;40:3229.
134. Chen WT, Yang KY, Wang CM, Huang YW, Sun G, Chiang ID, et al. High-efficiency broadband meta-hologram with polarization-controlled dual images. *Nano Lett.* 2014;14:225–30.
135. Chen X, Huang L, Mühlenbernd H, Li G, Bai B, Tan Q, et al. Dual-polarity plasmonic metalens for visible light. *Nat Commun.* 2012;3:1198.
136. Khorasaninejad M, Chen WT, Zhu AY, Oh J, Devlin RC, Rousso D, et al. Multispectral chiral imaging with a metalens. *Nano Lett.* 2016;16:4595–600.
137. Chen X, Chen M, Mehmood MQ, Wen D, Yue F, Qiu CW, Zhang S. Longitudinal multifoci metalens for circularly polarized light. *Adv Opt Mater.* 2015;3:1201–6.
138. Wang S, Wang X, Kan Q, Ye J, Feng S, Sun W, et al. Spin-selected focusing and imaging based on metasurface lens. *Opt Express.* 2015;23:26434–41.
139. Bai GD, Ma Q, Li RQ, Mu J, Jing HB, Zhang L, Cui TJ. Spin-symmetry breaking through metasurface geometric phases. *Phys Rev Appl.* 2019;12: 044042.
140. Gou Y, Ma HF, Wu LW, Wang ZX, Xu P, Cui TJ. Broadband spin-selective wavefront manipulations based on Pancharatnam-Berry coding metasurfaces. *ACS Omega.* 2021;6:30019–26.
141. Ji R, Xie X, Guo X, Zhao Y, Jin C, Song K, Wang S, Yin J, Liu Y, Jiang C, et al. Chirality-assisted Aharonov-Anandan geometric-phase metasurfaces for spin-decoupled phase modulation. *ACS Photonics.* 2021;8:1847–55.
142. Ji R, Song K, Guo X, Xie X, Zhao Y, Jin C, Wang S, Jiang C, Yin J, Liu Y, et al. Spin-decoupled metasurface for broadband and pixel-saving polarization rotation and wavefront control. *Opt Express.* 2021;29:25720–30.
143. Song Q, Odeh M, Zúñiga-Pérez J, Kanté B, Genevet P. Plasmonic topological metasurface by encircling an exceptional point. *Science.* 2021;373:1133–7.
144. Fu P, Du S, Lan W, Hu L, Wu Y, Li Z, Huang X, Guo Y, Zhu W, Li J, Liu B, Gu C. Deep learning enabled topological design of exceptional points for multi-optical-parameter control. *Commun Phys.* 2023;6:254.
145. Li Y, Wan S, Deng S, Deng Z, Lv B, Guan C, Yang J, Bogdanov A, Belov P, Shi J. Independent control of circularly polarized light with exceptional topological phase coding metasurfaces. *Photonics Res.* 2024;12:534–42.
146. Yang Z, Huang PS, Lin YT, Qin H, Zúñiga-Pérez J, Shi Y, Wang Z, Cheng X, Tang MC, Han S, et al. Creating pairs of exceptional points for arbitrary polarization control: asymmetric vectorial wavefront modulation. *Nat Commun.* 2024;15:232.
147. Yang Z, Huang PS, Lin YT, Qin H, Chen J, Han S, Huang W, Deng ZL, Li B, Zúñiga-Pérez J, et al. Asymmetric Full-Color Vectorial Meta-holograms Empowered by Pairs of Exceptional Points. *Nano Lett.* 2024;24:844–51.
148. Liu L, Zhang X, Kenney M, Su X, Xu N, Ouyang C, Shi Y, Han J, Zhang W, Zhang S. Broadband metasurfaces with simultaneous control of phase and amplitude. *Adv Mater.* 2014;26:5031–6.
149. Wang Q, Zhang X, Xu Y, Gu J, Li Y, Tian Z, Singh R, Zhang S, Han J, Zhang W. Broadband metasurface holograms: toward complete phase and amplitude engineering. *Sci Rep.* 2016;6:32867.
150. Liu W, Li Z, Li Z, Cheng H, Tang C, Li J, Chen S, Tian J. Energy-tailorable spin-selective multifunctional metasurfaces with full Fourier components. *Adv Mater.* 2019;31:1901729.
151. Zhao R, Xiao X, Geng G, Li X, Li J, Li X, Wang Y, Huang L. Polarization and Holography Recording in Real-and k-Space Based on Dielectric Metasurface. *Adv Funct Mater.* 2021;31:2100406.
152. Deng L, Deng J, Guan Z, Tao J, Chen Y, Yang Y, Zhang D, Tang J, Li Z, Li Z, Yu S, Zheng G, Xu H, Qiu CW, Zhang S. Malus-metasurface-assisted polarization multiplexing Light. *Sci Appl.* 2020;9:101.
153. Wan X, Jia SL, Cui TJ, Zhao YJ. Independent modulations of the transmission amplitudes and phases by using Huygens metasurfaces. *Sci Rep.* 2016;6:25639.
154. Shan X, Deng L, Dai Q, Zhou Z, Liang C, Li Z, Zheng G. Silicon-on-insulator based multifunctional metasurface with simultaneous polarization and geometric phase controls. *Opt Express.* 2020;28:26359–69.
155. Li Y, Pang Y, Wang J, Zheng Q, Zhang J, Zhang J, Jing Y, Zheng L, Feng M, Wang H, Qu S, Cui T. Tailoring Circular Dichroism in an Isomeric Manner: Complete Control of Amplitude and Phase for High-Quality Hologram and Beam Forming. *Adv Opt Mater.* 2022;10:2101982.
156. Rubin NA, Zaidi A, Dorrah AH, Shi Z, Capasso F. Jones matrix holography with metasurfaces. *Sci Adv.* 2021;7:eabg7488.
157. Nan T, Zhao H, Guo J, Wang X, Tian H, Zhang Y. Generation of structured light beams with polarization variation along arbitrary spatial trajectories using tri-layer metasurfaces. *Opto-Electron Sci.* 2024;3:230052–61.
158. Yue Z, Sipahi T, Ahmed H, Ansari MA, Wang G, Hou G, Chen X, Yang X. Multispectral Polarization States Generation with a Single Metasurface. *Laser Photonics Rev.* 2024;18:2400176.
159. Intaravanne Y, Wang R, Ahmed H, Ming Y, Zheng Y, Zhou ZK, Li Z, Chen S, Zhang S, Chen X. Color-selective three-dimensional polarization structures. *Light: Sci Appl.* 2022;11:302.
160. Zheng C, Li J, Liu J, Li J, Yue Z, Li H, Yang F, Zhang Y, Zhang Y, Yao J. Creating longitudinally varying vector vortex beams with an all-dielectric metasurface. *Laser Photonics Rev.* 2022;16:2200236.
161. Wang D, Liu F, Liu T, Sun S, He Q, Zhou L. Efficient generation of complex vectorial optical fields with metasurfaces. *Light: Sci Appl.* 2021;10:67.
162. Dorrah AH, Rubin NA, Zaidi A, Tamagnone M, Capasso F. Metasurface optics for on-demand polarization transformations along the optical path. *Nat Photonics.* 2021;15:287–96.

163. Dorrah AH, Rubin NA, Tamagnone M, Zaidi A, Capasso F. Structuring total angular momentum of light along the propagation direction with polarization-controlled meta-optics. *Nat Commun.* 2021;12:6249.
164. Liu W, Wang B, Zhang Y, Wang J, Zhao M, Guan F, Liu X, Lei S, Zi J. Circularly polarized states spawning from bound states in the continuum. *Phys Rev Lett.* 2019;123: 116104.
165. Zhen B, Hsu CW, Lu L, Stone AD, Soljačić M. Topological nature of optical bound states in the continuum. *Phys Rev Lett.* 2014;113: 257401.
166. Gorkunov MV, Antonov AA, Kivshar YS. Metasurfaces with maximum chirality empowered by bound states in the continuum. *Phys Rev Lett.* 2020;125: 093903.
167. Chen W, Yang Q, Chen Y, Liu W. Extremize optical chiralities through polarization singularities. *Phys Rev Lett.* 2021;126: 253901.
168. Li Z, Liu W, Li Z, Tang C, Cheng H, Li J, Chen X, Chen S, Tian J. Tripling the capacity of optical vortices by nonlinear metasurface. *Laser Photonics Rev.* 2018;12:1800164.
169. Ma M, Li Z, Liu W, Tang C, Li Z, Cheng H, Li J, Chen S, Tian J. Optical information multiplexing with nonlinear coding metasurfaces. *Laser Photonics Rev.* 2019;13:1900045.
170. Li G, Zhang S, Zentgraf T. Nonlinear photonic metasurfaces. *Nat Rev Mater.* 2017;2:1–14.
171. Hong X, Wang K, Guan C, Han X, Chen Y, Qian S, Xing X, Qiu CW, Lu P. Chiral third-harmonic metasurface for multiplexed holograms. *Nano Lett.* 2022;22:8860–6.
172. Wang M, Li Y, Tang Y, Chen J, Rong R, Li G, Cao T, Chen S. Nonlinear Chiroptical Holography with Pancharatnam-Berry Phase Controlled Plasmonic Metasurface. *Laser Photonics Rev.* 2022;16:2200350.
173. Mao N, Tang Y, Jin M, Zhang G, Li Y, Zhang X, Hu Z, Tang W, Chen Y, Liu X, Li K, Cheah K, Li G. Nonlinear wavefront engineering with metasurface decorated quartz crystal. *Nanophotonics.* 2021;11:797–803.
174. Kruk SS, Wang L, Sain B, Dong Z, Yang J, Zentgraf T, Kivshar Y. Asymmetric parametric generation of images with nonlinear dielectric metasurfaces. *Nat Photonics.* 2022;16:561–5.
175. Kim KH, Kim JR. Dielectric Chiral Metasurfaces for Second-Harmonic Generation with Strong Circular Dichroism. *Ann Phys.* 2020;532:2000078.
176. Walter F, Li G, Meier C, Zhang S, Zentgraf T. Ultrathin nonlinear metasurface for optical image encoding. *Nano Lett.* 2017;17:3171–5.
177. Almeida E, Bitton O, Prior Y. Nonlinear metamaterials for holography. *Nat Commun.* 2016;7:12533.
178. Ye W, Zeuner F, Li X, Reineke B, He S, Qiu CW, Liu J, Wang Y, Zhang S, Zentgraf T. Spin and wavelength multiplexed nonlinear metasurface holography. *Nat Commun.* 2016;7:11930.
179. Nookala N, Lee J, Tymchenko M, Gomez-Diaz JS, Demmerle F, Boehm G, Lai K, Shvets G, Amann MC, Alu A, Belkin M. Ultrathin gradient nonlinear metasurface with a giant nonlinear response. *Optica.* 2016;3:283–8.
180. Klein MW, Enkrich C, Wegener M, Linden S. Second-harmonic generation from magnetic metamaterials. *Science.* 2006;313:502–4.
181. Kang L, Rodrigues SP, Taghinejad M, Lan S, Lee KT, Liu Y, Werner DH, Urbas A, Cai W. Preserving spin states upon reflection: linear and nonlinear responses of a chiral meta-mirror. *Nano Lett.* 2017;17:7102–9.
182. Tang Y, Intaravanne Y, Deng J, Li KF, Chen X, Li G. Nonlinear vectorial metasurface for optical encryption. *Phys Rev Appl.* 2019;12: 024028.
183. Mao N, Deng J, Zhang X, Tang Y, Jin M, Li Y, Liu X, Li K, Cao T, Cheah K, Wang H, Ng J, Li G. Nonlinear diatomic metasurface for real and Fourier space image encoding. *Nano Lett.* 2020;20:7463–8.
184. Sun Y, Geng G, Wang Y, Zhang Y, Li Z, Liu W, Cheng H, Chen S. Multichannel Linear and Nonlinear Information Encryptions with Malus Metasurfaces. *Laser Photonics Rev.* 2024;18:2300866.
185. Arbabi E, Kamali SM, Arbabi A, Faraon A. Full-Stokes imaging polarimetry using dielectric metasurfaces. *ACS Photonics.* 2018;5:3132–40.
186. Yang Z, Wang Z, Wang Y, Feng X, Zhao M, Wan Z, Zhu L, Liu J, Huang Y, Xia J, Wegener M. Generalized Hartmann-Shack array of dielectric metalens sub-arrays for polarimetric beam profiling. *Nat Commun.* 2018;9:4607.
187. Rubin NA, D'Aversa G, Chevalier P, Shi Z, Chen WT, Capasso F. Matrix Fourier optics enables a compact full-Stokes polarization camera. *Science.* 2019;365:eaax1839.
188. Zhang X, Yang S, Yue W, Xu Q, Tian C, Zhang X, Plum E, Zhang S, Han J, Zhang W. Direct polarization measurement using a multiplexed Pancharatnam-Berry metahologram. *Optica.* 2019;6:1190–8.
189. Basiri A, Chen X, Bai J, Amrollahi P, Carpenter J, Holman Z, Wang C, Yao Y. Nature-inspired chiral metasurfaces for circular polarization detection and full-Stokes polarimetric measurements. *Light: Sci Appl.* 2019;8:78.
190. Ni Y, Chen C, Wen S, Xue X, Sun L, Yang Y. Computational spectropolarimetry with a tunable liquid crystal metasurface. *eLight.* 2022;2:23.
191. Yue F, Aglieri V, Piccoli R, Macaluso R, Toma A, Morandotti R, Razzari L. Highly Sensitive Polarization Rotation Measurement through a High-Order Vector Beam Generated by a Metasurface. *Adv Mater Tech.* 2020;5:1901008.
192. Yang B, Ma D, Liu W, Choi DY, Li Z, Cheng H, Tian J, Chen S. Deep-learning-based colorimetric polarization-angle detection with metasurfaces. *Optica.* 2022;9:217–20.
193. Fan Q, Xu W, Hu X, Zhu W, Yue T, Yan F, Lin P, Chen L, Song J, Lezec HJ, Agrawal A, Lu Y, Xu T. Disordered metasurface enabled single-shot full-Stokes polarization imaging leveraging weak dichroism. *Nat Commun.* 2023;14:7180.
194. Panchenko E, Cadusch JJ, James TD, Roberts A. Plasmonic metasurface-enabled differential photodetectors for broadband optical polarization characterization. *ACS Photonics.* 2016;3:1833–9.
195. Hong J, Van De Groep J, Lee N, Kim SJ, Lalanne P, Kik PG, Brongersma ML. Nonlocal metasurface for circularly polarized light detection. *Optica.* 2023;10:134–41.
196. Wilson NC, Shin E, Bangle RE, Nikodemski SB, Vella JH, Mikkelsen MH. Ultrathin Pyroelectric Photodetector with Integrated Polarization-Sensing Metasurface. *Nano Lett.* 2023. <https://doi.org/10.1021/acs.nanolett.3c02341>.
197. Wei J, Chen Y, Li Y, Li W, Xie J, Lee C, Novoselov KS, Qiu CW. Geometric filterless photodetectors for mid-infrared spin light. *Nat Photonics.* 2023;17:171–8.

198. Li W, Coppens ZJ, Besteiro LV, Wang W, Govorov AO, Valentine J. Circularly polarized light detection with hot electrons in chiral plasmonic metamaterials. *Nat Commun.* 2015;6:8379.
199. Zheng G, Mühlender H, Kenney M, Li G, Zentgraf T, Zhang S. Metasurface holograms reaching 80% efficiency. *Nat Nanotech.* 2015;10:308–12.
200. Zhang J, Elkabbash M, Wei R, Singh SC, Lam B, Guo C. Plasmonic metasurfaces with 42.3% transmission efficiency in the visible. *Light: Sci Appl.* 2019;8:53.
201. Luo W, Sun S, Xu HX, He Q, Zhou L. Transmissive ultrathin Pancharatnam-Berry metasurfaces with nearly 100% efficiency. *Phys Rev Appl.* 2017;7: 044033.
202. Arbabi A, Arbabi E, Horie Y, Kamali SM, Faraon A. Planar metasurface retroreflector. *Nat Photonics.* 2017;11:415–20.
203. Wu Z, Zhou M, Khoram E, Liu B, Yu Z. Neuromorphic metasurface. *Photonics. Research.* 2020;8:46–50.
204. Zhou C, Lee WB, Park CS, Gao S, Choi DY, Lee SS. Multifunctional beam manipulation at telecommunication wavelengths enabled by an all-dielectric metasurface doublet. *Adv Opt Mater.* 2020;8:2000645.
205. Zang H, Xi Z, Zhang Z, Lu Y, Wang P. Ultrasensitive and long-range transverse displacement metrology with polarization-encoded metasurface. *Sci Adv.* 2022;8:eadd1973.
206. Menzel C, Helgert C, Rockstuhl C, Kley EB, Tünnermann A, Pertsch T, Lederer F. Asymmetric transmission of linearly polarized light at optical metamaterials. *Phys Rev Lett.* 2010;104: 253902.
207. Li Z, Chen S, Tang C, Liu W, Cheng H, Liu Z, Li J, Yu P, Xie B, Liu Z, Li J, Tian J. Broadband diodelike asymmetric transmission of linearly polarized light in ultrathin hybrid metamaterial. *Appl Phys Lett.* 2014;105: 201103.
208. Zhang C, Pfeiffer C, Jang T, Ray V, Junda M, Upreti P, Podraza N, Grbic A, Guo LJ. Breaking Malus' law: highly efficient, broadband, and angular robust asymmetric light transmitting metasurface. *Laser Photonics Rev.* 2016;10:791–8.
209. Li Z, Liu W, Cheng H, Liu J, Chen S, Tian J. Simultaneous generation of high-efficiency broadband asymmetric anomalous refraction and reflection waves with few-layer anisotropic metasurface. *Sci Rep.* 2016;6:35485.
210. Frese D, Wei Q, Wang Y, Huang L, Zentgraf T. Nonreciprocal asymmetric polarization encryption by layered plasmonic metasurfaces. *Nano Lett.* 2019;19:3976–80.
211. Zhou Y, Kravchenko II, Wang H, Nolen JR, Gu G, Valentine J. Multilayer noninteracting dielectric metasurfaces for multiwavelength metaoptics. *Nano Lett.* 2018;18:7529–37.
212. Ding J, Xu N, Ren H, Lin Y, Zhang W, Zhang H. Dual-wavelength terahertz metasurfaces with independent phase and amplitude control at each wavelength. *Sci Rep.* 2016;6:34020.
213. Zhou Y, Kravchenko II, Wang H, Zheng H, Gu G, Valentine J. Multifunctional metaoptics based on bilayer metasurfaces. *Light: Sci Appl.* 2019;8:80.
214. Wang X, Ding J, Zheng B, An S, Zhai G, Zhang H. Simultaneous realization of anomalous reflection and transmission at two frequencies using bi-functional metasurfaces. *Sci Rep.* 2018;8:1876.
215. Cai T, Wang GM, Xu HX, Tang SW, Li H, Liang JG, Zhuang YQ. Bifunctional Pancharatnam-Berry Metasurface with High-Efficiency Helicity-Dependent Transmissions and Reflections. *Ann Phys.* 2018;530:1700321.
216. Pan W, Cai T, Tang S, Zhou L, Dong J. Trifunctional metasurfaces: concept and characterizations. *Opt Express.* 2018;26:17447–57.
217. Jing Y, Li Y, Zhang J, Wang J, Feng M, Ma H, Qu S. Full-space-manipulated multifunctional coding metasurface based on "Fabry-Pérot-like" cavity. *Opt Express.* 2019;27:21520–31.
218. Gao S, Zhou C, Liu W, Yue W, Chen S, Lee SS, Choi DY, Li Y. Dielectric Polarization-Filtering Metasurface Doublet for Trifunctional Control of Full-Space Visible Light. *Laser Photonics Rev.* 2022;16:2100603.
219. Deng J, Gao F, Yuan P, Li Y, Yan B. Bidirectional nanoprinting based on bilayer metasurfaces. *Opt Express.* 2022;30:377–88.
220. Fang Q, Wu L, Pan W, Li M, Dong J. Trifunctional metasurface for manipulating linearly and circularly polarized waves in transmission and reflection modes. *Appl Phys Lett.* 2020;117: 074102.
221. Cai T, Wang G, Tang S, Xu H, Duan J, Guo H, Guan F, Sun S, He Q, Zhou L. High-efficiency and full-space manipulation of electromagnetic wave fronts with metasurfaces. *Phys Rev Appl.* 2017;8: 034033.
222. Deng J, Li Z, Zhou Z, He Z, Zeng Y, Zheng G, Yu S. Bilayer-Metasurface Design, Fabrication, and Functionalization for Full-Space Light Manipulation. *Adv Opt Mater.* 2022;10:2102179.
223. Yuan Y, Zhang K, Ratni B, Song Q, Ding X, Wu Q, Burokur SN, Genevet P. Independent phase modulation for quadruplex polarization channels enabled by chirality-assisted geometric-phase metasurfaces. *Nat Commun.* 2020;11:4186.
224. Liu Z, Li Z, Liu Z, Cheng H, Liu W, Tang C, Gu C, Li J, Chen H-T, Chen S, Tian J. Single-layer plasmonic metasurface half-wave plates with wavelength-independent polarization conversion angle. *ACS Photonics.* 2017;4:2061–9.
225. Deng ZL, Deng J, Zhuang X, Wang S, Li K, Wang Y, Chi Y, Ye X, Xu J, Wang GP, Zhao R, Wang X, Cao Y, Cheng X, Li G, Li X. Diatomic metasurface for vectorial holography. *Nano Lett.* 2018;18:2885–92.
226. Wu PC, Tsai WY, Chen WT, Huang YW, Chen TY, Chen JW, Liao CY, Chu CH, Sun G, Tsai DP. Versatile polarization generation with an aluminum plasmonic metasurface. *Nano Lett.* 2017;17:445–52.
227. Ding J, An S, Zheng B, Zhang H. Multiwavelength metasurfaces based on single-layer dual-wavelength meta-Atoms: toward complete phase and amplitude modulations at two wavelengths. *Adv Opt Mater.* 2017;5:1700079.
228. Wang C, Wang C. Interference-enhanced chirality-reversible dichroism metalens imaging using nested dual helical surfaces. *Optica.* 2021;8:502–10.
229. Cao Y, Tang L, Li J, Lee C, Dong ZG. Four-channel display and encryption by near-field reflection on nanoprinting metasurface. *Nanophotonics.* 2022;11:3365–74.
230. Bao Y, Yu Y, Xu H, Guo C, Li J, Sun S, Zhou ZK, Qiu CW, Wang XH. Full-colour nanoprint-hologram synchronous metasurface with arbitrary hue-saturation-brightness control. *Light Sci & Appl.* 2019;8:95.
231. Wang S, Deng ZL, Wang Y, Zhou Q, Wang X, Cao Y, Guan BO, Xiao S, Li X. Arbitrary polarization conversion dichroism metasurfaces for all-in-one full Poincaré sphere polarizers. *Light Sci Appl.* 2021;10:24.

232. Fan Q, Liu M, Zhang C, Zhu W, Wang Y, Lin P, Yan F, Chen L, Lezec HJ, Lu Y, Agrawal A, Xu T. Independent amplitude control of arbitrary orthogonal states of polarization via dielectric metasurfaces. *Phys Rev Lett*. 2020;125:267402.
233. Liu M, Zhu W, Huo P, Feng L, Song M, Zhang C, Chen L, Lezec HJ, Lu Y, Agrawal A, Xu T. Multifunctional metasurfaces enabled by simultaneous and independent control of phase and amplitude for orthogonal polarization states. *Light: Sci Appl*. 2021;10:107.
234. Guo X, Zhong J, Li P, Wen D, Liu S, Wei B, Qi S, Zhao J. Metasurface-assisted multidimensional manipulation of a light wave based on spin-decoupled complex amplitude modulation. *Opt Lett*. 2022;47:353–6.
235. Gao S, Zhou C, Yue W, Li Y, Zhang C, Kan H, Choi DY. Efficient all-dielectric diatomic metasurface for linear polarization generation and 1-bit phase control. *ACS Appl Mater Interfaces*. 2021;13:14497–506.
236. Song Q, Khadir S, Vézian S, Damilano B, Mierry PD, Chenot S, Brandli V, Genevet P. Bandwidth-unlimited polarization-maintaining metasurfaces. *Sci Adv*. 2021;7:eabe1112.
237. Ma D, Li Z, Zhang Y, Liu W, Cheng H, Chen S, Tian J. Giant spin-selective asymmetric transmission in multipolar-modulated metasurfaces. *Opt Lett*. 2019;44:3805.
238. Li H, Xu H, Zheng C, Liu J, Li J, Song C, Li J, Yang F, Shi W, Zhang Y, Zhang Y, Yao J. All-Silicon Diatomic Terahertz Metasurface with Tailorable Linear Polarization States. *Adv Optical Mater*. 2023;11:2201960.
239. Chen J, Yu F, Liu X, Bao Y, Chen R, Zhao Z, Wang J, Wang X, Liu W, Shi Y, Qiu CW, Chen X, Lu W, Li G. Polychromatic full-polarization control in mid-infrared light. *Light Sci Appl*. 2023;12:105.
240. Liu W, Wang B, Zhang Y, Wang J, Zhao M, Guan F, Liu X, Shi L, Zi J. Circularly polarized states spawning from bound states in the continuum. *Phys Rev Lett*. 2019;123:116104.
241. Zhao R, Wei Q, Li Y, Li X, Geng G, Li X, Li J, Wang Y, Huang L. Stereo Jones Matrix Holography with Longitudinal Polarization Transformation. *Laser Photonics Rev*. 2023;17:2200982.
242. Dai C, Liu T, Wang D, Zhou L. Multiplexing near- and far-field functionalities with high-efficiency bi-channel metasurfaces. *Photonix*. 2024;5:11.
243. Shi Z, Rubin NA, Park JS, Capasso F. Nonseparable polarization wavefront transformation. *Phys Rev Lett*. 2022;129:167403.
244. Deng ZL, Tu QA, Wang Y, Wang ZQ, Shi T, Feng Z, Qiao XC, Wang GP, Xiao S, Li X. Vectorial compound metapixels for arbitrary nonorthogonal polarization steganography. *Adv Mater*. 2021;33:2103472.
245. Sun S, Ma HF, Gou Y, Zhang TY, Wu LW, Cui TJ. Spin-and Space-Multiplexing Metasurface for Independent Phase Controls of Quadruplex Polarization Channels. *Adv Opt Mater*. 2023;11:2202275.
246. Dong S, Qu K, Hu Q, Wang S, Chen K, Feng Y. Full-Space Janus Meta-Lens for Shared-Aperture Transmission-Reflection-Independent Focusing of Electromagnetic Wave. *Adv Photonics Res*. 2024;5:2300349.
247. Zhang X, Liu Y, Han J, Kivshar Y, Song Q. Chiral emission from resonant metasurfaces. *Science*. 2022;377:1215–8.
248. Sun Y, Hu Z, Shi K, Guo T, Xing Y, Jin Y, He S. Enhancing circularly polarized emission by a planar chiral dielectric metasurface. *Adv Opt Mater*. 2023;11:2300197.
249. Qu Y, Yi S, Yang L, Yu Z. Multimodal light-sensing pixel arrays. *Appl Phys Lett*. 2022;121:040501.
250. Shen Z, Zhao F, Jin C, Wang S, Cao L, Yang Y. Monocular metasurface camera for passive single-shot 4D imaging. *Nat Commun*. 2023;14:1035.
251. Zhao Y, Xiang J, He A, He Y, Guo X, Su Y. Metamaterial-enabled Fully On-Chip Polarization-Handling Devices. *Laser Photonics Rev*. 2023;17:2300320.
252. Zhang Y, Li Z, Liu W, Cheng H, Choi DY, Tian J, Chen S. On-Chip Multidimensional Manipulation of Far-Field Radiation with Guided Wave-Driven Metasurfaces. *Laser Photonics Rev*. 2023;17:2300109.
253. Zhang Y, Li Z, Liu W, Li Z, Cheng H, Chen S, Tian J. Spin-selective and wavelength-selective demultiplexing based on waveguide-integrated all-dielectric metasurfaces. *Adv Optical Mater*. 2019;7:1801273.
254. Huang H, Overvig AC, Xu Y, Malek SC, Tsai CC, Alù A, Yu N. Leaky-wave metasurfaces for integrated photonics. *Nat Nanotechnol*. 2023;18:580–8.
255. Ji J, Wang Z, Sun J, Chen C, Li X, Fang B, Zhu SN, Li T. Metasurface-Enabled On-Chip Manipulation of Higher-Order Poincaré Sphere Beams. *Nano Lett*. 2023;23:2750–7.
256. Xu G, Overvig A, Kasahara Y, Martini E, Maci S, Alù A. Arbitrary aperture synthesis with nonlocal leaky-wave metasurface antennas. *Nat Commun*. 2023;14:4380.
257. Chen T, Xu M, Pu M, Zeng Q, Zheng Y, Xiao Y, Ha Y, Guo Y, Zhang F, Chi N, Luo X. Freeform Metasurface-Assisted Waveguide Coupler for Guided Wave Polarization Manipulation and Spin–Orbit Angular Momentum Conversion. *ACS Photonics*. 2024;11:1051–9.
258. Zhao X, Li Z, Cheng J, Liu W, Yu S, Zhang Y, Cheng H, Tian J, Chen S. Realization of maximum optical intrinsic chirality with bilayer polyatomic metasurfaces. *Opt Lett*. 2022;47:4814–7.
259. Deng ZL, Hu MX, Qiu S, Wu X, Overvig A, Li X, Alù A. Poincaré sphere trajectory encoding metasurfaces based on generalized Malus' law. *Nat Commun*. 2024;15:2380.

## Publisher's Note

Springer Nature remains neutral with regard to jurisdictional claims in published maps and institutional affiliations.